DESIGN AND ANALYSIS OF PHOTONIC CRYSTAL FIBER BASED BIO-CHEMICAL SENSORS

SUBMITTED IN PARTIAL FULFILLMENT OF THE REQUIREMENTS

FOR THE AWARD OF THE DEGREE

OF

MASTER OF SCIENCE

IN

PHYSICS

Submitted by:

NEERAJ SINGH

2K22/MSCPHY/27

Under the supervision of

DR AJEET KUMAR

DEPARTMENT OF APPLIED PHYSICS

DELHI TECHNOLOGICAL UNIVERSITY

(Formerly Delhi College of Engineering)

Bawana Road, Delhi – 110042

June-2024

DEPARTMENT OF APPLIED PHYSICS

DELHI TECHNOLOGICAL UNIVERSITY

(Formerly Delhi College of Engineering)

Bawana Road, Delhi 110042

CANDIDATE'S DECLARATION

I, **Neeraj Singh,** hereby certify that the work which is being presented in the thesis entitled **"Design and Analysis of Photonic Crystal Fiber Based Bio-Chemical Sensors"** in partial fulfilment of the requirements for the Degree of Master of Science, submitted to the Department of Applied Physics, Delhi Technological University, is an authentic record of my own work carried out during the period from 2022 To 2024 under the supervision of Dr. Ajeet Kumar.

The matter presented in the thesis has not been submitted by me for the award of any other degree of this or any other institute.

1. Title of the Paper: Design and analysis of a rectangular core refractive index-based PCF sensor for bio-sensing application

Author names (in the sequence as per research paper): Neeraj Singh, Akash Khamaru and Ajeet Kumar

Name of: Name of the Journal: Optical and Quantum Electronics

Status of paper (Accepted/ Published/ Communicated): Accepted and Published

Date of paper communication: 4 March 2024

Date of Acceptance: 11 May 2024

2. Title of the Paper: Design and analysis of a rectangular Core Photonic Crystal Fiber biosensor based on Terahertz regime for malaria detection

Author names (in the sequence as per research paper): Neeraj Singh and Ajeet Kumar

Name of Conference: International Conference on Atomic, Molecular, Material, Nano, and Optical Physics with Applications (ICAMNOP-2023)

Name of the Journal: Springer Nature Proceedings of ICAMNOP-2023 (Scopus Indexed)

Conference Dates with venue: December 20th-22nd, 2023; Delhi Technological University, Delhi, India

Have you registered for the conferences: Yes

Status of paper (Accepted/ Published/ Communicated): Accepted

Date of paper communication: March, 2024

This is to certify that the student has incorporated all the corrections suggested by the examiners in the thesis and the statement made by the candidate is correct to the best of our knowledge.

Place: Delhi   **Neeraj Singh**

Date: 07/06/2024   (2K22/MSCPHY/27)

Signature of Supervisor

DEPARTMENT OF APPLIED PHYSICS

DELHI TECHNOLOGICAL UNIVERSITY

(Formerly Delhi College of Engineering)

Bawana Road, Delhi-110042

CERTIFICATE

Certified that **Neeraj Singh** (2K22/MSCPHY/27) has carried out their research work presented in this thesis entitled **"Design And Analysis Of Photonic Crystal Fiber Based Bio-Chemical Sensors"** for the award of **Master of Science** from Department of Applied Physics, Delhi Technological University, Delhi, under my supervision. The thesis embodies results of original work, and the studies carried out by the student himself and the contents of the thesis do not form the basis of award of any other degree to the candidate or to anybody else from this or any other University/Institution.

Place: Delhi

DR AJEET KUMAR

Date: 07/06/2024

ACKNOWLEDGEMENT

ABSTRACT

This work proposes highly sensitive Photonic Crystal Fiber based terahertz sensors for bio-chemical sensing applications. The proposed sensors function as refractive index sensors, capable of detecting changes in refractive index with exceptional sensitivity. All the fibers are simulated computationally on Finite Element Method (FEM) based COMSOL Multiphysics software. In this research work we have designed rectangular core PCF with rectangular air holes and Zeonex as background material, working in terahertz frequency range. Various performance parameters were numerically analysed such as relative sensitivity, confinement loss, effective mode index, effective mode area, non-linearity, and birefringence. With the proposed designs high relative sensitivity, low confinement loss, and high birefringence have been reported around the frequency range of 0.5 THz to 1.5 THz. The high sensitivity values suggest that proposed design has significant potential for detecting various types of cancer cells, blood components detection, malaria detection and many other types of biomolecules detection. Additionally, various fabrication processes are suggested to enable the production of these fibers for real-world applications.

CONTENTS

1.6.1 Dispersion

1.6.1.1 Intermodal Dispersion
1.6.1.2 Intramodal Dispersion

1.6.2 Attenuation

1.6.2.1 Absorptive losses
1.6.2.2 Radiative losses

2.1.1 Solid Core
2.1.2   Hollow core
2.1.3 Porous core

3.1.1 Effective mode index
3.1.2 Confinement loss
3.1.3 Effective mode area
3.1.4 Effective material loss

LIST OF FIGURES

LIST OF TABLES

LIST OF ABBREVIATIONS

RI   Refractive Index

FEM   Finite Element Method

TIR   Total Internal Reflection

ME   Maxwell's Equation

RIP   Refractive Index Profile

SMF   Single Mode Fiber

EM   Electromagnetic

TE   Transverse Electric

TM   Transverse Magnetic

PCF   Photonic Crystal Fiber

CL   Confinement Loss

EMA   Effective mode area

NA   Numerical Aperture

PDE   Partial Differential Equation

SPR   Surface Plasmon Resonance

SPW   Surface Plasmon Wave

SPP   Surface Plasmon Polariton

PML   Perfectly matched layer

FBG   Fiber Bragg Grating

CHAPTER-1

INTRODUCTION

1.1 HISTORY

Our present world runs on information, a lot data and information is generated worldwide per second and this creates a demand for transmission of information. Scientist and engineers are continuously trying to evolve new technologies to increase the capacity of information transmission and enhance light wave communication. The different components of a communication system are semiconductor laser diode (coherent source providing a carrier wave for carrying information), a transmission channel (Optical fiber), and a receiver consisting of an optical detector and associated electronics for signal retrieving [1]. In a lightwave communication system, the core element is optical fiber, which serves as a transmission channel that conveys the light beam carrying data. Light is guided through the optical fiber using the phenomenon of Total Internal Reflection. In 19th century, Researchers such as John Tyndall and Alexander Graham Bell experimented with transmission of light through transparent materials, laying the groundwork for the concept of optical communication. Early 20th century and a number of attempts are being made to transmit images through optical fibers but these systems have very limited performance and practicality. The invention of lasers in 1960s opened the doors for fiber optics as lasers provided a highly focused and intense source of light suitable for efficient transmission through optical fibers. A paper was published by Charles K.kao and George A. Hockham in 1966 proposing the use of optical
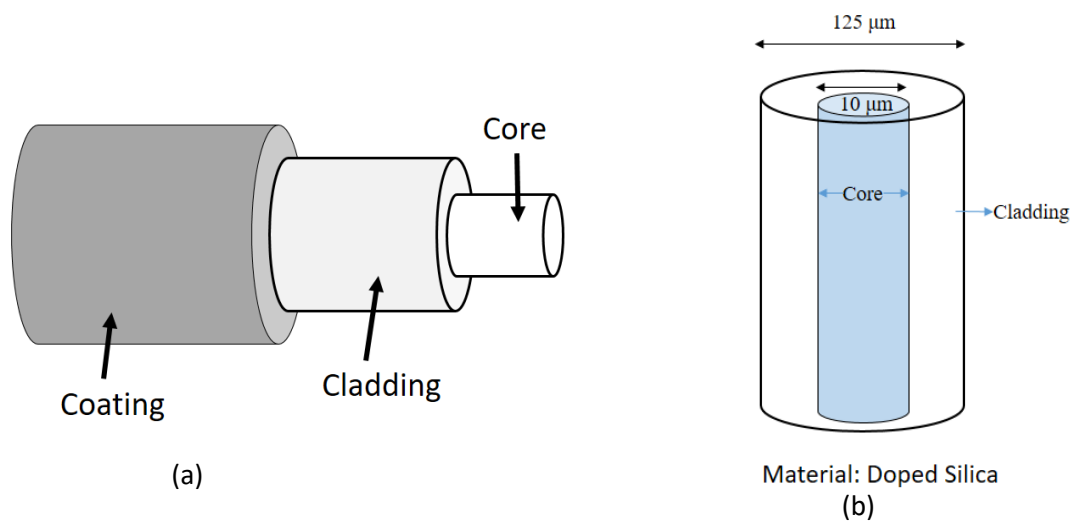
Fig 1.1 (a) Components of a fiber, (b) Single mode fiber

fibers for long distance communication, which outlined the use of glass fibers for low-loss transmission of light [2]. The steep fall in loss in the early 1970s, with the advancement of technology Corning glass works in the United States developed a low loss optical fiber (20dB/km at the He-Ne laser wavelength of 633 nm) that paved a way for practical use of the optical fibers as a transmission medium in lightwave communication systems. 1970-1980 this decade saw the commercialisation of fiber optic cables and systems.

Currently, a variety of optical fibres are available, however single mode fibres are the most commonly utilised with a core diameter of about 10μm with an overall diameter of 125 μm usually made of doped silica as shown in fig. 1.1. Dopants are added to the silica to provide a radial variation in the refractive index (RI). Silica fiber has a very low loss at 1500nm wavelength and zero dispersion at 1300nm wavelength. Optical fibers are the backbone of global communication network and have revolutionised the field of telecommunication. An optical fiber is a structure which guides a beam of light from one place to another. Optical fibers can be put into different categories on the basis of following parameters: (i) Structure: cylindrical, planar, strip and birefringent, (ii) Refractive index Profile (RIP): step index and graded index fibers, (iii) Number of modes: Single mode and multimode fibers, (iv) Dispersion: natural, dispersion shifted, reverse dispersion and dispersion winded fibers, (v) Polarization, (vi) On the basis of signal proceeding ability [3].

1.2 PROPAGATION OF LIGHT IN FIBERS

Analysis of propagation of light in the fibers is done by two approaches: a) ray analysis b) electromagnetic or modal analysis. Ray analysis is suitable for primitive treatments but when applied to more complex problems, particularly those involving narrowband, coherent light, ray analysis may lead incorrect conclusions. Modal analyses begin by utilizing the differential Maxwell's equations (MEs), integrating the boundary conditions set by the fiber, and deriving all feasible solutions [4]. Solution of these Maxwell's equation are called **modes or optical modes** of the fiber. Among these solutions important solutions are those which are guided by the fiber's core. These modes are of utmost relevance for both physics and engineering applications, as they are both finite and discrete solutions. In mathematical terms, the modes are eigenfunctions, also known as eigenmodes or eigensolutions, of the system governed by Maxwell's equations and the refractive index profile (RIP). The Electromagnetic (EM) waves travelling through optical fiber has three different modes: (i) Transverse Electric (TE), (ii)

Transverse Magnetic(TM) and, (iii) Hybrid modes (having both axial and magnetic electric fields E_z and H_z)[5]. Hybrid modes are further categorized into EH and HE modes.

Based on guiding region modes can be classified into three categories:

1. Core modes, discrete and finite in number, are the modes guided by core cladding interface.

2. Cladding modes are guided by the interfaces between the core and cladding, as well as between the cladding and buffer. These modes are discrete and limited in number.

3. Radiation modes are solutions to Maxwell's equations that are not confined within the fiber. These modes are infinite.
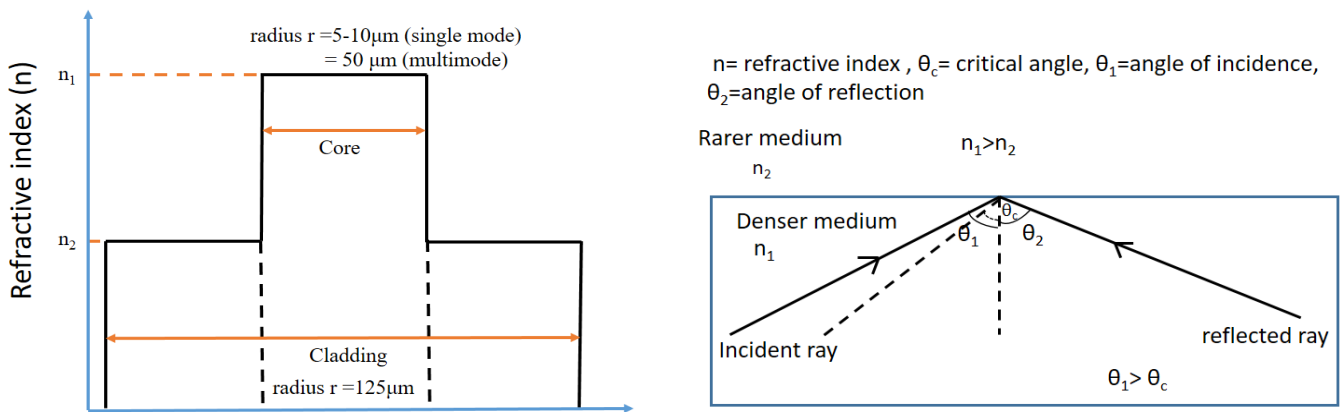
Fig 1.2 (a) Refractive Index Profile of step index fiber, (b) Total Internal Reflection

1.3 STEP INDEX FIBER

Step index fiber has a dielectric cylindrical core and a dielectric cladding of slightly lower refractive index. Step-index fibers exhibit a uniform RIP throughout the core, with a sudden decrease in the RI at the cladding. Fig. 1.2(a) shows the refractive index profile of the Step Index Fiber. The light is guided though the core using the phenomenon of successive total internal reflection. Fig 1.2(b) shows the Total internal reflection phenomenon on the boundary of two medium . Total internal reflection (TIR) is a phenomenon in which light waves travelling from a medium 1 with a higher refractive index (n1) to a medium 2 with a lower refractive index (n2) are completely reflected back when the angle of incidence is higher than a certain angle (at medium 1 and 2 interface) called critical angle θ_c.

$$\theta_c = \sin^{-1} \frac{n_2}{n_1} \tag{1.1}$$

1.4 GRADED INDEX FIBER

In graded index fiber the RI of the core is maximum on the axis and decreases as we move away from the axis and becomes constant in the cladding. Fig 1.3 depicts the parabolic RIP for a graded index fiber.
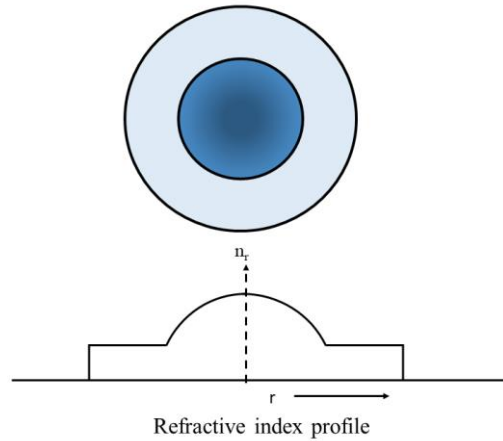
Fig. 1.3 Parabolic refractive index profile of a Graded index fiber

1.5 SINGLE MODE AND MULTIMODE FIBERS

Single Mode Fibers (SMFs) has a core diameter of 5-10 µm with an overall diameter of 125 µm including cladding. Due to small size of the core single solution if MEs or mode is guided through the fiber in the axis parallel to the fiber. SMFs are used in long distance telecommunication. On the other hand multimode fibers have a core diameter of 50-62.5 µm and overall diameter same as single mode fiber, 125 µm including cladding. Multiple core guided modes are allowed in multimode fiber. These fibers are used in short distance communications such as video surveillance and local area network. Fig. 1.4 (a,b) shows the propagation of light through a single mode fiber and a multimode fiber. The optical parameter that determine fiber is a single mode fiber or multi-mode fiber is known as "V parameter", which is given by [6]:

$$V = \frac{2\pi}{\lambda} r (n_{co}^2 - n_{cl}^2)^{1/2} \tag{1.2}$$

Here, r is the core's radius, λ is the wavelength of light and n_{co} and n_{cl} are RIs of core and cladding respectively.

4

Now if V≤ 2.405, the fiber is SMF and if V≥2.405, the fiber is multimode fiber.
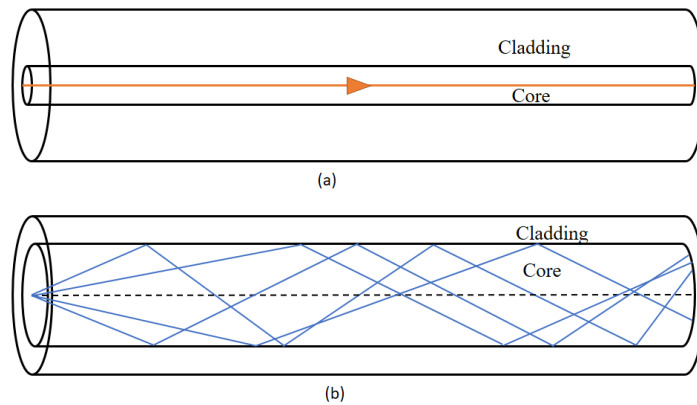
Fig 1.4 (a) Single mode fiber, (b) Multimode fiber

1.6 ATTENUATION AND DISPERSION IN OPTICAL FIBERS

Attenuation and dispersion are important characters of an optical fiber which determines the cost of telecommunication system, as they determine the repeater spacing in telecommunication systems that are needed to maintain acceptable signal level.

1.6.1 Dispersion

Pulse dispersion determines the information carrying capacity of fiber as it limits fiber's bandwidth. Light pulse transmitted into a fiber spreads as it propagates through the fibers, this broadening is called dispersion. There are two types of dispersion: (i) Intermodal dispersion and (ii) Intramodal dispersion.

1.6.1.1 Intermodal Dispersion

Intermodal dispersion, as the name suggests, is a phenomena that occurs in an optical fibre between various modes. Thus, this dispersion category is limited to multimode fibre. As different rays or modes takes different time to propagate through a particular length of the fiber. As different rays travel different optical path length, those traverse a longer length take longer time to reach the output end. Consequently broadening of pulse takes place and different pulses spread into one another. Therefore, even if two pulses are well resolved at the input end, they may not remain resolved at the output end. If the output pulses are not distinguishable, no information can be retrieved. Hence Multimode fiber's bandwidth and data transfer distance are restricted by this effect.

1.6.1.2 Intramodal Dispersion

Intramodal dispersion is of two types: waveguide dispersion and material dispersion. Material dispersion is due to the intrinsic properties of the material of optical fiber, because of these intrinsic properties light of different wavelengths propagates with different velocities in the optical fiber. The RI varies with wavelength. This applies to both single mode and multimode fibers. Waveguide dispersion is significant only in single mode fibers.

1.6.2 Attenuation

Because of absorption and scattering losses, the amount of light power that travels through a fibre decreases exponentially with length. There are two broad sources of attenuation in an optical fiber and categorized as: absorptive and radiative losses.

1.6.2.1 Absorptive losses

Absorptive losses can be intrinsic and extrinsic losses. Intrinsic losses are due to interaction of light waves with fiber's material for example glass. One of the example of such interaction is infrared absorption band of silica. The tails of absorption bands in the far infrared and ultraviolet are responsible for the tiny absorption losses of pure silica in the near infrared and visible ranges. Extrinsic absorption losses are caused by impurities. Impurities like transition metal ions and hydroxyl ion dissolved in glass in very small amount account for absorption losses.

1.6.2.2 Radiative losses

Radiative losses occur due to coupling of guided light modes and radiation modes due to scattering. The coupling leads to the loss of energy. The unavoidable Rayleigh scattering is responsible for such coupling which is caused by small scale inhomogeneities frozen into the fiber. These inhomogeneities arises during fabrication process of the fiber which results in composition and density fluctuations. Rayleigh scattering losses are proportional to λ^{-4}. Fiber bending and imperfections in fiber such as diameter fluctuation, core cladding irregularities, also leads to radiative losses.

CHAPTER 2

PHOTONIC CRYSTAL FIBER

Photonic Crystal fiber (also known as Holey fiber or Microstructured fibers) is an optical fiber which consist periodic arrangement of air holes or low index inclusion which go through the whole length of the fiber. Photonic crystal fiber (PCF) derives its waveguide properties not from the spatial variation in glass composition, but from the arrangement of numerous tiny, closely spaced air holes.The shape, arrangement and size of these holes largely affect the properties of these fibers.PCF was invented by Philip Russell in late 1990s and was first explored in 1996 at University of Bath. Photonic crystal fibers have numerous advantages over conventional fibers e.g., high tensile strength, low absorption loss, large bandwidth, flexibility, and very low confinement loss. Photonic crystal fiber also have an ability to confine light in hollow cores, creating a photonic band gap, not possible in conventional optical fiber. Hence Photonic Crystal Fiber have two modes of operations: index guiding and photonic band gap. Earlier, PCFs were utilized in the communications sector to enable faster data transmission with enhanced security. With advancement in technology PCF are now employed in numerous promising applications in our daily life such as fiber lasers, nonlinear devices, high-power transmission, highly sensitive sensors, and supercontinuum generation.
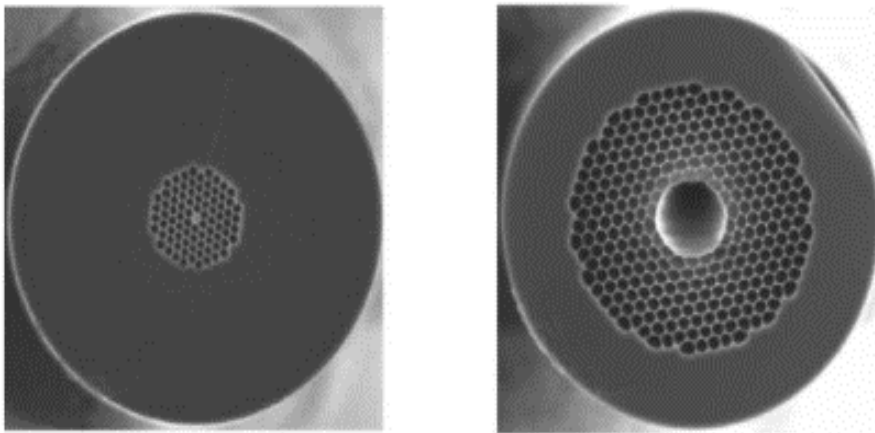
Fig 2.1- Photonic Crystal Fiber Cross-section [7]

2.1 TYPES OF PHOTONIC CRYSTAL FIBER

Similar to the step index fibers, photonic crystal fiber can be single mode and multimode. These single mode or multimode fibers can be further classified on the basis of nature of their core.

2.1.1 Solid Core

Solid core fiber is characterized by a core with a higher average RI than that of the cladding. In photonic crystal fiber the core and the cladding material is same characterized by the symmetric configuration of air holes. Solid core photonic crystal fiber operates on the principle of TIR, as the core possesses a higher refractive index compared to the effective refractive index of the cladding.
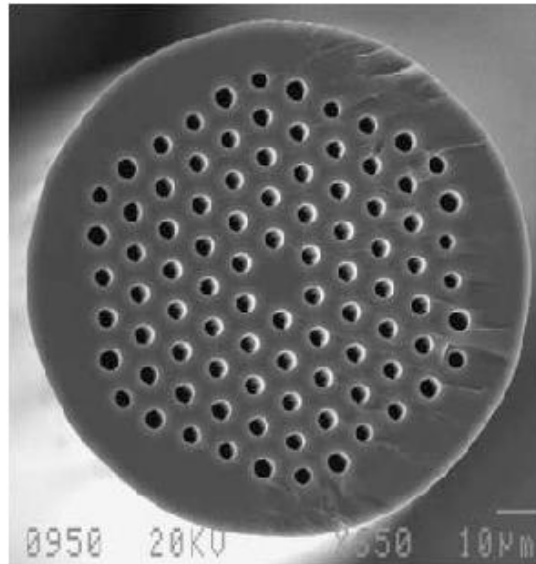
Fig 2.2-Solid core Photonic crystal fiber made of silica glass with hexagonal patterned air holes [8]

2.1.2 Hollow Core

Hollow core photonic crystal fiber are based on guiding light through a rarer medium. The refractive index of the core in hollow core fiber is less than the cladding region, mostly it is a air hole. The core acts as a defect which creates a region through which light of a particular frequency range can pass through, called Photonic band gap.
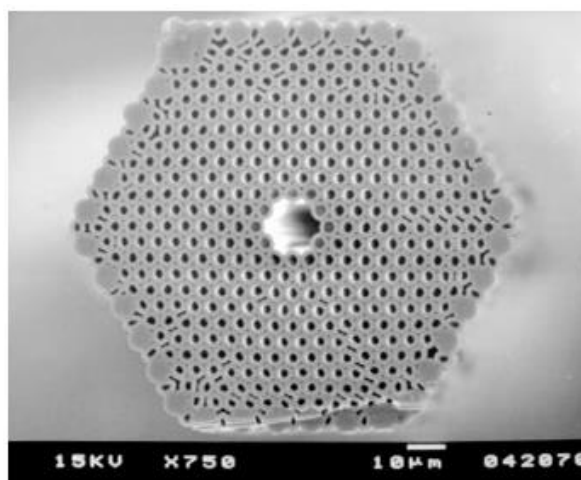
Fig 2.3 Hollow core Photonic crystal fiber [9]

8

2.1.3 Porous Core

A porous core PCF refers to a specific type of optical fiber that has a core with a porous structure. This design involves introducing pores or voids into the core of the fiber, creating a microstructure that can affect the way light propagates through the fiber. The core of the fiber contains a network of pores or voids. The arrangement and size of these pores can be carefully designed to achieve specific optical properties.
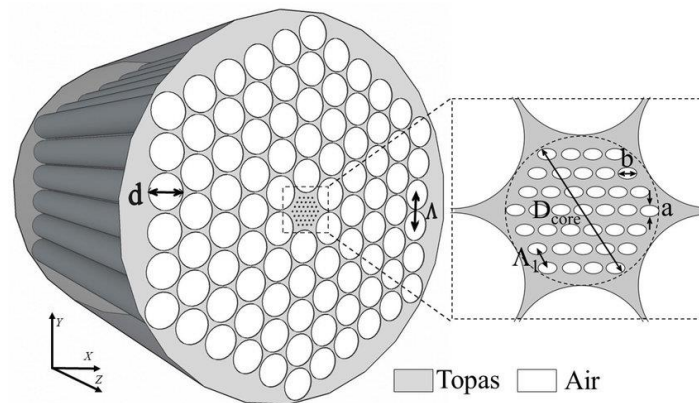
Fig 2.4 Porous core photonic crystal fiber [10]

2.2 MODES OF OPERATION

Light is guided through PCF mainly by two principles: Total internal reflection and Photonic band gap. In solid core or liquid core PCF light is directed through fiber by modified TIR if the average RI of the cladding is less than RI of the core, which means positive RI difference between core and cladding. Alternative solid core PCF and liquid core PCF configurations are known to guide via a photonic bandgap generated by the cladding. These types of structures are typically identified by a cladding that has isolated inclusions with a higher index. These inclusions can be created by up-doped regions inside the glass or polymer host or by a liquid with the proper RI [11]. Hollow core PCF uses photonic bandgap to guide light and in the absence of bandgap, light is guided by inhibited coupling between core modes and coupling modes [12, 13]. Photonic band gap fiber is characterised by low attenuation over a narrow wavelength range determined by the bandgap while the inhibited coupling fiber exhibits somewhat higher propagation loss yet guides over considerably broader wavelength ranges.

2.3 ADVANTAGES OF PCF

Compact size, light weight, tunable optical parameters, polarization control are some of the advantages of a photonic crystal fiber. Tunable optical parameter is one of the most important feature of a PCF as it allows for precise control over the propagation of light. By carefully

designing the crystal lattice, researchers can engineer specific optical properties, such as dispersion, nonlinearity, and birefringence. This flexibility enables customization for various applications. Also PCF can be designed to control the polarization of light which makes useful in application such as polarization maintaining fiber. PCF fibers has two modes of operation or guiding mechanism: (i) TIR, (ii) Photonic band gap. This versatility of guiding mechanism makes PCF useful for a wide range of application including non- linear optics.

2.4 APPLICATIONS OF PCF

PCF has a wide range of application in a variety of field as Scientists, engineers, and designers make use of their distinctive features. Some of the applications of PCF are described below.

1. Telecommunication- PCF are used for high speed data transmission in telecommunication networks. Due to its distinct optical properties, several channels at various wavelength can be sent over a single fiber in Wavelength Division Multiplexing Systems.

2. Non-linear Optics- The behavior of a medium is influenced by the intensity of light. Up to a specific threshold frequency, the material exhibits linear properties; however, beyond this threshold frequency, the medium begins to exhibit nonlinear behavior. Supercontinuum generation arises from the interaction of these nonlinear effects in response to an intense input light pulse.

3. Fiber lasers and amplifiers-PCF are used to construct high power fiber lasers. The unique properties of PCFs helps in improving laser performance. PCFs are also used as amplifying wires in optical amplifiers which helps in enhancing the performance of communication system.

4. Sensing- PCF fibers are used in used in sensors as both sensing element and as data transmitter. PCF sensor can be used for physical and bio-chemical sensing. Physical sensor include pressure senor, temperature sensor, stress and strain sensor, hence finding their application in structural monitoring, industrial production monitoring, automation, environmental analysis etc. Biochemical sensors are used for sensing of ph level, various types of chemicals and biological substances including protein, blood glucose, ethanol, urea, cancer cells, DNA, RNA investigation etc. hence finding its use in biomedical sciences and chemical sciences.

2.5 FABRICATION

Photonic crystal fibers have a relatively complex structure. The symmetric air holes and size of the fiber makes it relatively hard to fabricate the PCFs. But with the advancement in technology and introduction of new equipment now it is possible to fabricate more and more complex structure. There are various techniques available to fabricate a PCF like stack and draw [14], capillary stacking, gas pressurization, sol-gel [15], extrusion [16], and 3D printing [17]. 3D printing being a relatively new technology can be used to fabricate symmetric and asymmetric designs with different shape air holes like rectangular, elliptical and circular etc. Fig. 2.5 shows the preform containing silica capillaries stacked hexagonally.
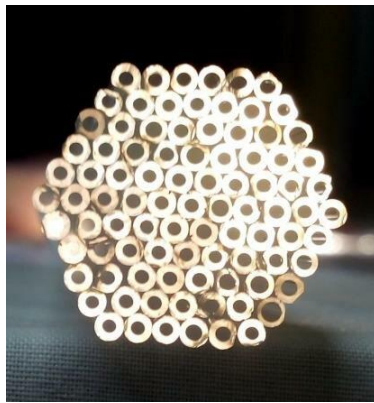
Fig 2.5 : (a) Preform containing hexagonally stacked silica capillaries [18]

CHAPTER-3

OPTICAL PROPERTIES AND SIMULATION

3.1 PROPERTIES DEFINING A PCF

There are various optical properties or parameters that are used to define an optical fiber. These properties include confinement loss, effective mode area, effective material loss, birefringence, Non-linearity, power fraction, and numerical aperture.

3.1.1 Effective Mode Index

Light propagating through the fiber encounters an average refractive index determined by the design of the photonic crystal fiber. This average refractive index is referred to as the effective mode index. It can be evaluated using [19]:

$$n_{eff} = \frac{\beta}{k_o} \qquad (3.1)$$

3.1.2 Confinement Loss

The confinement loss depicts the radiation confinement in the core. Due to various factors light energy escapes from the core, confinement loss is a measure of this power loss. It is a crucial parameter for evaluating the fibers performance. The lower the confinement loss, more will be the confining ability of the fiber.

Confinement loss is analysed as [20]:-

$$CL\left(\frac{dB}{cm}\right) = 8.868 \times k_o \times l_m\big(n_{eff}\big) \times 10^{-2} \qquad (3.2)$$

Here k_o is the propagation constant, $l_m(n_{eff})$ is the imaginary part of the effective RI.

3.1.3 Effective Mode Area

The Effective Mode Area (EMA) of a PCF sensor defines its key sensing zone. Spatial distribution of the guided optical mode is attributed by effective mode area. Effective area is given by [21],

$$\text{EMA} = \frac{\left(\iint |E|^2 \, dxdy\right)^2}{\iint |E|^4 \, dxdy} \qquad (3.3)$$

Here, E is the electric field.

3.1.4 Effective material loss

Effective material loss is the total material loss due to material absorption and scattering within the fiber core and cladding. By calculating the ratio of the integral over the fibre's dielectric material to the integral over the entire fibre cross-section, we can determine the amount of radiation absorbed by the fiber. It can be calculated by [22]:

$$\alpha_{eff} = \sqrt{\frac{\varepsilon_o}{\mu_o}} \left(\frac{\int_{mat} n_{mat} \alpha_{mat} |E|^2 dxdy}{|\int_{all} P_z dA|} \right) \tag{3.4}$$

Where, n_{mat} is the RI of background material and α_{mat} represents material absorption loss of respective material. ε_0, μ_0 is the relative permittivity and permeability in the free space respectively. E and S_z represents the electric field and poynting vector's z component accordingly.

3.1.5 Birefringence

In sensing application utilizing PCFs, achieving high birefringence is crucial. Maintaining polarization is essential to counteract the detrimental effect of polarization mode dispersion and to ensure stable operation of the PCF [23]. Birefringence is the absolute value of difference in refractive index of two x and y polarization modes [24].

$$B = |n_{eff}^x - n_{eff}^y| \tag{3.5}$$

3.1.6 Non-linearity

It quantifies the strength of non-linear effect. Non-linearity is the variation in refractive index with respect to intensity of light. Non-linearity can be calculated using [25]:

$$\Upsilon = \frac{2\pi}{\lambda} \left(\frac{n_2}{EMA} \right) \tag{3.6}$$

Here, n_2 is non-linear refractive index, EMA is effective mode area.

3.1.7 Power fraction

Power fraction reflects the light hold by the fiber. Power fraction is given by [26]:

$$P = \frac{sample \int R(E_x H_y - E_y H_x) dxdy}{whole \int R(E_x H_y - E_y H_x) dxdy} \times 100\% \tag{3.7}$$

Where E_x, E_y and H_x, H_y is the electric and magnetic field direction in X and Y direction respectively. The numerator gives the quantity of light transmitting through the fiber's core and denominator is light transmission through whole fiber.

3.1.8 Numerical aperture

The observation of radiation acceptance or emission by the core involves the computation of the numerical aperture (NA). Numerical aperture can be calculated as [27]:-

$$NA = \frac{1}{\sqrt{1 + \frac{\pi A_{eff}}{\lambda^2}}} \tag{3.8}$$

Here, A_{eff} is the EMA and λ is the wavelength of the incident light.

3.2 SIMULATION

The rapid advancement of technology has fostered the continuous emergence of innovative ideas globally. Notably, the field of optics has experienced exponential growth over the past few decades, leading to the introduction of novel fiber designs and applications. In our increasingly computational world, the initial analysis and performance evaluation of optical fibers are predominantly conducted through computational simulations using specialized software before physical fabrication.

Multiphysics software such as COMSOL Multiphysics, RP Fiber, and Ansys Multiphysics are instrumental in simulating fiber designs and assessing their performance. These simulations allow for a comprehensive analysis of fiber properties and behavior under various conditions. Furthermore, the capability of simulation software extends to the evaluation of theoretical fiber designs that may not yet be feasible to fabricate, providing valuable insights and guiding future developments. This approach not only enhances the efficiency of the design process but also ensures that innovative fiber technologies are thoroughly vetted for performance and viability prior to fabrication.

3.2.1 COMSOL Multiphysics Software

COMSOL Multiphysics is a finite element analysis and simulation software package designed for a broad spectrum of physics and engineering applications, particularly coupled phenomena and multiphysics. The software supports traditional physics-based user interfaces as well as linked systems of partial differential equations (PDEs). COMSOL provides an integrated

development environment and a single workflow for electrical, mechanical, hydraulic, acoustics, optical, and chemical applications.

In addition to addressing classical problems with application modules, the core Multiphysics package is capable of solving PDEs. An API for Java, along with LiveLink for MATLAB and LiveLink products for major CAD software, allows for external control of the software. The Application Builder enables the creation of custom domain-specific simulation applications, utilizing either drag-and-drop tools (Form Editor) or programming (Method Editor). COMSOL Server is a dedicated software for managing COMSOL simulation applications within organizations. Numerous modules are available, categorized by application areas such as Electrical, Mechanical, Fluid, Acoustic, Chemical, Multipurpose, and Interfacing.

Fig 3.1 COMSOL Multiphysics software

3.3 NUMERICAL ANALYSIS

Simulation software is equipped with advanced algorithms to numerically analyze proposed fiber designs and evaluate their performance. These tools utilize various mathematical methods to conduct comprehensive numerical analyses of optical fibers. Several of these methods are discussed below.

3.3.1 Finite Element Method

The finite element method (FEM) is a numerical technique employed to obtain approximate solutions for boundary value problems associated with PDEs. It is also utilized for solving integral equations. FEM achieves this by partitioning a complex problem into smaller, more manageable components known as finite elements. The physical structure or domain is divided into a finite number of subdomains, called elements, which are interconnected at points called nodes. This process is known as meshing.

3.3.2 Finite Difference Time Domain Method

The Finite Difference Time Domain (FDTD) method, developed by A. Thom in 1920, is a computational technique used to simulate models in one, two, and three dimensions. Initially created to address hydrodynamics problems, FDTD discretizes differential equations into difference equations using central difference approximations. These difference equations are then solved iteratively in a leapfrog manner. In this method, the value of the dependent variable at a specific point within the solution region is determined by its values at neighbouring points. The key steps involved in FDTD include:

1. Dividing the solution region into a grid of nodes, with a finer grid yielding more accurate results.
2. Approximating the given differential equation as a difference equation using central difference approximations, which relate the value of the dependent variable at a specific point to its values at neighbouring points.
3. Solving the resulting difference equation iteratively in a leapfrog manner, subject to the prescribed boundary conditions.

CHAPTER -4

PHOTONIC CRYSTAL FIBER SENSORS

Optical fibre sensor technology is a direct result of the industry revolutions in fibre optic communication and optoelectronics. Optical fiber sensor acts as both sensing element and also for signal transportation. Optical fiber sensor has many advantages over electrical sensors. Electrical sensors and Optical fiber sensors differ greatly in terms of sensing mode, sensing principle, signal transmission technique, signal survey, and signal disposition [28]. When compared to optical sensors, electronic sensors have a few key drawbacks, including higher assembly costs, intricate systems, slower reaction times, lower precision, and noise from temperature, impedance, and electromagnetic sources. PCF sensors being the optical fiber sensors inherits all the properties of optical fiber sensors and also includes their own characteristic properties. PCF sensors are compact, lightweight, resist EM interference, have large bandwidth, higher sensitivity, flexibility and environmental robustness, all these characteristics make these sensors quite useful in a variety of circumstances. Photonic crystal fibers are used to sense temperature and pressure, force, stress, humidity, ph, cancer cell, blood sugar, malaria voltage, current, magnetic field etc. Effective refractive index is an important factor which defines a Photonic crystal fiber and its related properties. Effective refractive index obtained in complex form and varies with frequency of light which in turn vary important optical properties such as confinement loss, effective mode area waveguide dispersion, propagation constant.

4.1 TERAHERTZ SENSORS

Terahertz sensors are refractive index sensors are primarily employed in biochemical sensing applications wherein the hollow core of the fiber is filled with a specific analyte. These sensors detect variations in the refractive index across a frequency range of 0.1×10^{12} Hz to 10×10^{12} Hz. Recently, terahertz sensors have garnered significant attention from the scientific community, particularly for applications in biochemical sensing, spectroscopy, biotechnology, and industrial processes. This interest is largely due to their unique advantages, including the low energy of terahertz frequency photons, which preserves the integrity of the test layer. Additionally, terahertz sensors are compact, robust, offer fast response times, pose low health risks due to their non-invasive nature, and feature a large filling area, with core radii and overall diameters greater than those of sensors operating in the infrared and mid-infrared ranges.

Notably, terahertz sensors have demonstrated higher sensitivity compared to their infrared and mid-infrared counterparts [29].

4.2 PLASMONIC PCF SENSORS

Plasmonic PCF sensors uses the principle of Surface Plasmon Resonance (SPR) to detect variation in refractive index of different analytes for sensing application. Free electrons in a thin metal conductor oscillates on metal-dielectric interface, upon absorbing light, known as plasma oscillations and the quanta of these oscillation is called Surface Plasmon Wave (SPW). Fiber is coated with a thin layer of Plasmonic metal. When light passes through the fiber it give rise to SPW which circulates along core cladding region [30]. At some frequency or wavelength the core mode couples with the Surface Plasmon Polariton (SPP) mode under phase matching condition called SPR and in this condition the SPW absorbs most of the energy of the incident light and resonance peak in the loss spectrum occurs [31]. SPR is very sensitive to the RI variation of the fiber. That is, the resonance condition occurs at completely different wavelength or frequency even if there is a very minute change in the refractive index and loss peak of the fiber. This shift in refractive index and loss peak is what which is measured. The RI change can be due to stress, strain, temperature change, change in refractive index of the analyte filled in the core. Mainly nanometric layer of Gold (Au), Silver (Ag) is used as Plasmonic material. PCF can be put into two categories on the basis of fabrication methodology: (i) Internal metal deposition (IMD), (ii) External metal deposition (EMD) (ii) D shaped PCF. In IMD technique, Plasmonic material layer is coated inside the air holes and in EMD technique the layer of Plasmonic material is coated outside the fiber material, analyte being in direct contact with it. The fiber's surface is finely polished in D-shaped PCF to create a flat surface [32]. PCF SPR allows for label free detection and non-invasive sensing.

4.3 INTERFEROMETRIC PCF SENSORS

Interferometric PCF sensors employ the core and cladding areas of a single core PCF as the interferometer's sensing and reference arms [33]. Dual- or multi-core PCFs utilise interference between fundamental modes of various cores, as well as interference between one core's fundamental modes and higher order modes [34, 35]. In PCF-based sensing applications, the length of the interferometer is determined by the length of the PCF. When the effective RI of the mode propagating through sensing arm is changed, phase of such sensing modes changes which leads to an optical path difference with the modes propagating in the reference arm. This results in a wavelength shift in the transmission spectrum which is measured.

4.4 FIBER BRAGGS GRATING BASED SENSORS

A fibre Bragg grating (FBG) is an optical structure where the fibre core's refractive index varies periodically. This modulation in RI causes light to be reflected at a certain wavelength, known as the Bragg wavelength λ_B, through Fresnel reflection. Hence grating behaves like a wavelength selective mirror. FBGs can be analyzed using coupled mode theory. In the context of modes, FBGs facilitate the coupling of different modes, both co-propagating and counter-propagating, thus transferring optical power from one mode to another. Power is transferred to counter- and co-propagating optical modes via short- and long-period gratings, respectively. Cladding modes can also be excited, allowing the fabrication of flexible optical sensor devices. Various structures can be used to create fiber Bragg gratings: (i) uniform FBG, characterized by a uniform positive-only index change; (ii) chirped FBG, where the grating period varies linearly; (iii) tilted FBG, with a refractive index variation angled relative to the optical axis; (iv) superstructure FBG, consisting of several small FBGs placed in close proximity; and (v) apodized FBG, which utilizes a graded refractive index

4.5 COATED PCF SENSORS

In addition to the metal coatings utilized for creating plasmonic PCFs, various other coatings can be employed for fiber sensing applications. Notably, graphene has been used due to its exceptional optoelectronic properties. Graphene layers or films has a two-dimensional structure, consisting of carbon material with a thickness of one atom. This makes graphene a highly promising candidate for various applications, including the development of innovative field-effect transistors and transparent conductive films. Consequently, graphene oxide is often considered a viable alternative, offering a balance between the desirable properties of graphene and the challenges associated with its synthesis and cost. A wide range biosensors, chemical sensors and gas sensors based on graphene oxide have been proposed. For instance, a graphene oxide coated PCF has been fabricated to create a modal Mach-Zehnder interferometer for strain and temperature sensing. The Mach-Zehnder interferometer behavior is achieved due to the difference in phase constants between the core and cladding modes.

CHAPTER -5

DESIGN AND ANALYSIS OF A RECTANGULAR CORE REFRACTIVE INDEX-BASED PCF SENSOR FOR BIO-SENSING APPLICATION[1]

5.1 INTRODUCTION

Photonic crystal fibers are attracting attention in the terahertz (THz) range for their unique capabilities in guiding and manipulating electromagnetic waves. Moreover, high sensitivity, compact size, low cost, flexibility, and fast response make them ideal for a variety of sensing applications [36]. Particularly, bio-chemical sensing which includes detecting or sensing of various biological components such as different types of cancer cells, blood components, analysis of RNA, DNA, and proteins and malaria cells. Utilizing the low photon energy within the THz range, THz sensors offer exceptional penetration capability through porous samples while maintaining test layer integrity [37]. Furthermore, PCFs operating in the THz range offer significant advantages in terms of sensing analyte due to their large filling area, as the diameter of air holes and fiber diameter is larger than PCFs that are being operated in the mid-infrared range [38]. Due to these properties, various THz sensors and detectors have been developed using PCF. Hollow core fibers offer higher sensitivity than solid core fibers. Hollow-core fibers (HCFs) exhibit superior suitability for detecting distinct analytes having lower RI and also offer strong light-analyte interaction within the core [39]. Compared to solid core or porous core PCF, HC-PCF has a larger core power fraction and a lower effective material loss since the core is only filled with the target analyte.

PCF is becoming an increasingly important component of contemporary biological and biomedical technology since it may be used to detect blood components and cancer cells in both invasive and non-invasive ways among other things. Numerous THz optical sensors have been documented for use in biological applications. The advantages of PCF enable researchers to test different models for the detection of different analytes. Arif et el. proposed a chemical sensor, having a hexagonal cladding with circular air holes for liquid sensing and attained a relative sensitivity value of 50%, 55.83%, and 59.07% for water, ethanol, and benzene,

respectively [20]. A chemical sensor with rotated hexacore and heptagonal cladding design with circular holes proposed by Selim Hossain et al. exhibit a relative sensitivity of 68.48%, 69.20%, 66.78%, for ethanol, benzene, and water analyte at 1THz [40]. Rahaman et al. suggested a dumbbell shaped HC-PCF with rectangular air holes for chemical sensing using TOPAS as the fiber material and achieved a relative sensitivity of 96.25% for Ethanol [41]. Ahmed et al. proposed a blood component sensor for analytes such as RBCs, hemoglobin, WBCs, plasma, and water and achieved a sensitivity response of 80.93%, 80.56%, 80.13%, 79.91% and 79.39% at frequency 1.5 THz [42] . Bulbul et al. investigated a general purpose biochemical sensor with rectangular air holes and obtained a relative sensitivity of 95.82% at 2.5THz [43].

In this chapter a refractive index sensor is proposed, the difference in refractive index is used for the identification of different analytes with RI ranging from 1.35 to 1.39. Zeonex is used as the background material. Zeonex is a transparent thermoplastic. It is preferred due to its wide range of optical characteristics, including its consistent refractive index of 1.53 in the THz regime, low absorption loss of 0.2 cm^{-1}, high glass transition temperature, minimal water absorption, high biocompatibility, and exceptional chemical resistance even at high temperatures [24]. Rectangular air holes are introduced in the fiber with a rectangular hollow core in which analytes are filled.

The chapter is categorised into 4 sections. Section 1 discusses previous research on different PCF sensors. Section 2 gives sensor design and different optical parameter definition. Section 3 presents the numerical results which gives the idea about performance of the proposed sensor. Section 4 gives the conclusion regarding the effectiveness of the proposed sensor.

5.2 SENSOR MODEL DESIGN

Fig. 5.1 displays the cross-sectional representation of the proposed PCF sensor. The rectangular air holes of different widths and heights are arranged across PCF. The overall diameter of the proposed design is 3.3mm. The Perfectly matched layer (PML) occupies the cladding area and serves as an artificial absorbing medium to absorb radiation energy at the outer surface in the computational area and the width of the PML is 165 μm. Within the domain, the complete mesh consists of 24,554 elements while along the boundary it comprises 2,452 elements. The width W1 and height H1 of the core is 400μm and 500μm respectively. Width W2 is 200 μm and H2 is 1540 μm respectively. Parameters W3 and W4 are 1720 μm and 1520 μm respectively. Parameters H2, H3, H4 are 1540 μm, 1340 μm, 1240 μm respectively. The pitch

(separation between two adjacent rectangles) is 20μm. The core is infiltrated with analyte samples with refractive index ranges from 1.35 to 1.39 serving as a region where light analyte interaction takes place. To begin the study, firstly the core of the PCF sensor is injected with the liquid analyte. Fig. 5.2 shows the light propagation through the core filled with analyte. Since very little light leaves the core region, there is very little loss.
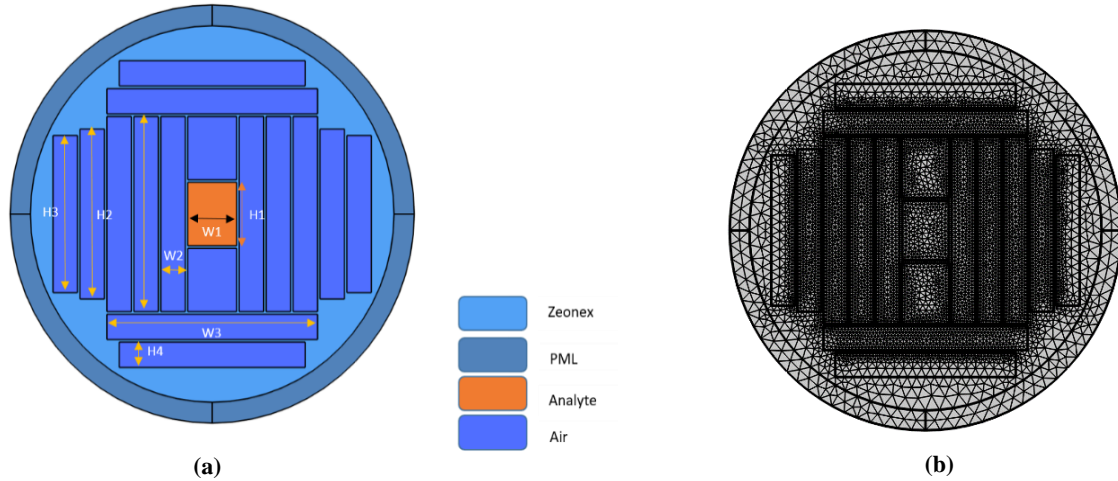

(a)   (b)

Fig. 5.1 (a) Sensor model design **(b)** meshing of proposed sensor

5.3 NUMERICAL ANALYSIS

As discussed in chapter 3, various optical parameters are evaluated to analyze the performance of the proposed sensor. These parameters include Relative sensitivity (RS), confinement loss (*CL*), power fraction, Non-linearity (*γ*), Effective mode area (EMA), and Birefringence. These parameters significantly impact the performance of the PCF sensors.

The RS is a crucial property that expresses the change in the optical response of the structure compared to the change in the external parameter. It measures the changes in the RI with the variation in the surroundings. It can be calculated using the following relation [44]:

$$RS = \frac{n}{n_{eff}} \times P \tag{5.1}$$

Here, *n* is the RI of the sensing analyte and *n_eff* is the effective mode index (EMI). Here *P* represents the power fraction.

As discussed in chapter 3, Power fraction (*P*) is calculated using the following equation,

$$P = \frac{sample \int R(E_x H_{y-} E_y H_x)dxdy}{whole \int R(E_x H_y - E_y H_x)dxdy} \times 100\% \tag{5.2}$$

EMI is evaluated using:

$$n_{eff} = \frac{\beta}{k_o} \tag{5.3}$$

Here, β is the normalised propagation constant, k_o represents wave number in vacuum.
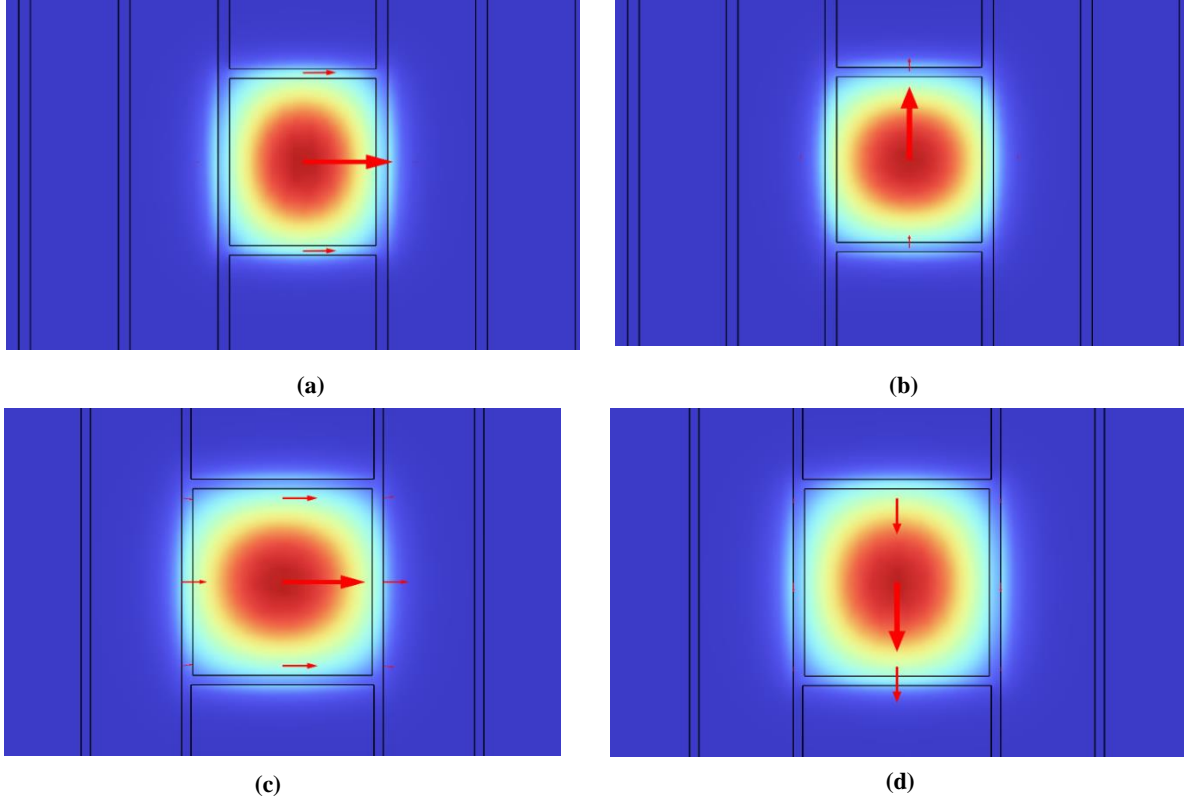

(a)

(b)

(c)

(d)

Fig. 5.2 (a), (b) Mode electric field distribution and **c**, **d** Mode magnetic field distribution of the proposed fiber for analyte with refractive index 1.39 at 1.4THz frequency in X and Y

Birefringence is evaluated using the following formula,

$$B = |n_{eff}^x - n_{eff}^y| \tag{5.4}$$

The optimal region for analyte sensing and the cross-sectional area that interacts with the light is the effective mode area. We can evaluate the effective mode area by the relation:

$$EMA = \frac{\left(\iint |E|^2 dxdy\right)^2}{\iint |E|^4 dxdy} \tag{5.5}$$

Here, |E| denotes the electric field distribution of the proposed fiber sensor.

Confinement loss is an important factor in analyzing the efficiency of an optical device, particularly in photonic crystal fibers. Minimum the value of CL better would be the transmission of light within the waveguide. CL is evaluated using:

$$CL\left(\frac{dB}{cm}\right) = 8.868 \times k_o \times l_m\left(n_{eff}\right) \times 10^{-2} \tag{5.6}$$

Here, k_o is the propagation constant, and $l_m(n_{eff})$ is the imaginary part of the effective refractive index of the propagating fundamental mode.

Non-linearity refers to the modifications in refractive index due to change in light intensity. By altering the parameters, a highly sensitive sensor can be designed to detect even subtle variations in the surrounding medium.

$$\Upsilon = \frac{2\pi}{\lambda}\left(\frac{n_2}{EMA}\right) \tag{5.7}$$

Where n_2 is non-linear refractive index and EMA is effective mode area.

5.4 RESULT AND DISCUSSION

To assess the guiding characteristics of the suggested rectangular core PCF, simulation and analysis are conducted using the FEM based COMSOL Multiphysics Software.
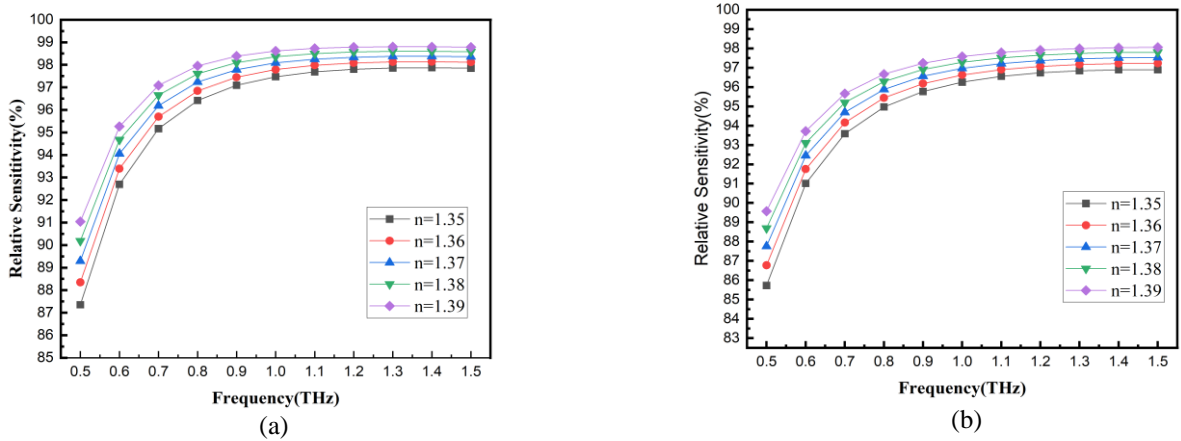

(a)

(b)

 Fig. 5.3 (a) and (b) Relative sensitivity variation with frequency in X and Y polarization directions respectively

Fig. 5.3 a, b shows relative sensitivity variation with frequency for different analytes with RI ranging from n=1.35 to 1.39. Relative sensitivity for analytes with higher refractive index is greater than for analytes with lower refractive index. We obtained relative sensitivity values 96.889%, 97.217%, 97.515%, 97.787%, 98.035% for RI of the analyte n=1.35, 1.36, 1.37, 1.38, 1.39 respectively in Y polarized direction at an operating frequency of 1.4THz. Relative sensitivity values of 97.868%, 98.135%, 98.378%, 98.599%, 98.800% are achieved for analyte with RI n=1.35, 1.36, 1.37, 1.38, 1.39 respectively in X polarized direction at an operating frequency of 1.4THz. These values indicate that there is an exceptionally high relative sensitivity obtained to all analyte samples.
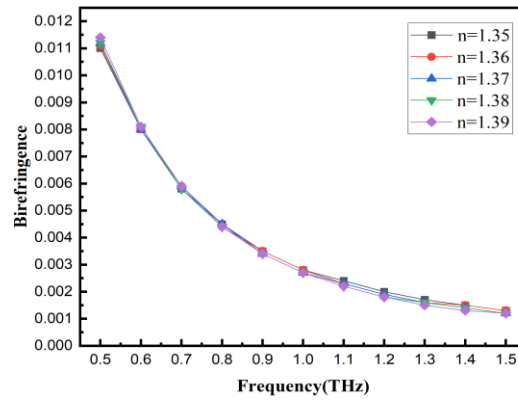
Fig 5.4 Birefringence variation with frequency

Fig. 5.4 shows birefringence of different analytes with RI, n= 1.35, 1.36, 1.37, 1.38, 1.39. Birefringence decreases with increase in frequency. Birefringence values achieved for analytes with RI, n=1.35, 1.36, 1.37, 1.38, 1.39 are 0.0015, 0.0015, 0.0014, 0.0014 and 0.0013 respectively at 1.4THz operating frequency.
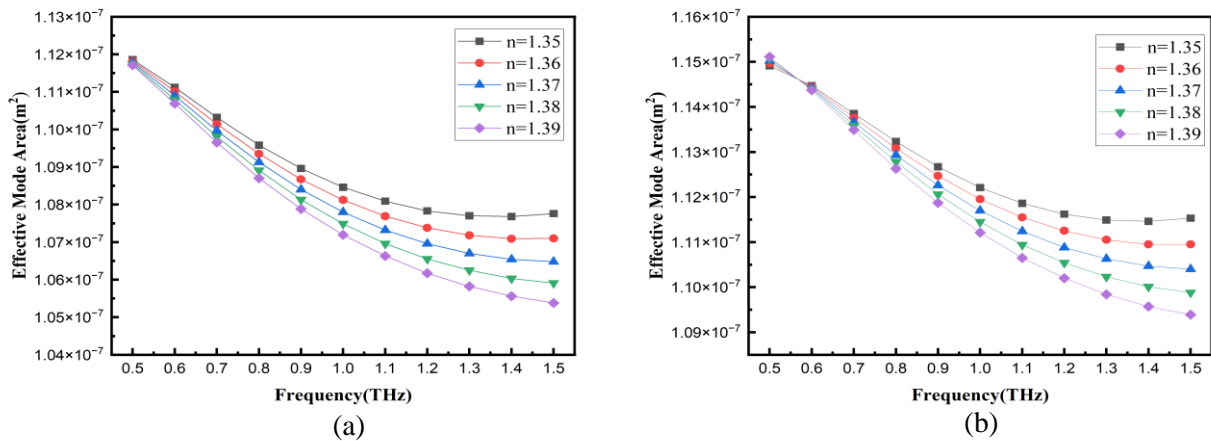

(a)	(b)

Fig. 5.5 a and **b** Effective mode area variation with frequency in X and Y polarization directions respectively

Fig. 5.5(a, b) shows the EMA profile achieved for different analytes within the 1.35-1.39 RI range for X and Y polarization directions. With the increase in the frequency of light, there is a decrease in the EMA of the fiber. Higher frequencies mean shorter wavelengths and shorter wavelengths can be easily confined in the fiber. We achieved an average effective mode area of order 10^{-7} m^2. At 1.4THz frequency effective mode area is $1.1146 \times 10^{-7} m^2$, $1.1095 \times 10^{-7} m^2$, $1.1047 \times 10^{-7} m^2$, $1.1001 \times 10^{-7} m^2$, $1.0957 \times 10^{-7} m^2$ for an analyte with RI, n=1.35, 1.36, 1.37, 1.38, 1.39 respectively with Y polarization of electric field. In X polarized direction we

observed an effective mode area of $1.0768 \times 10^{-7} m^2$, $1.0709 \times 10^{-7} m^2$, $1.0654 \times 10^{-7} m^2$, $1.0603 \times 10^{-7} m^2$, $1.0556 \times 10^{-7} m^2$ for an analyte with RI, n=1.35, 1.36, 1.37, 1.38, 1.39 respectively.
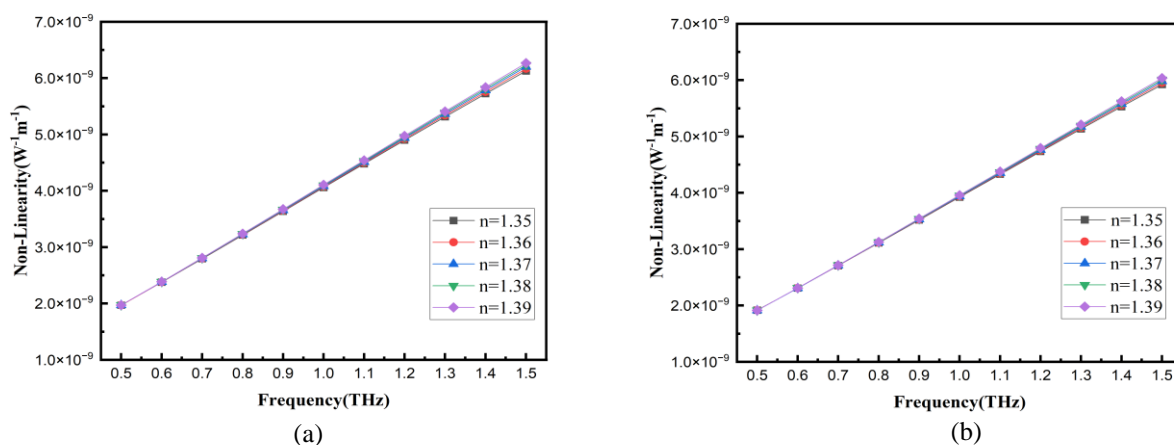

(a) (b)

Fig. 5.6 Non-Linearity variation with frequency **(a)** X, **(b)** Y polarization direction respectively

Fig. 5.6 (a, b) shows the non-linearity variation for both X and Y polarization directions in frequency range of 0.5–1.5 THz. Non-linearity increases linearly with frequency. We achieved non-linearity values of 5.528×10^{-9} $W^{-1}m^{-1}$, 5.553×10^{-9} $W^{-1}m^{-1}$, 5.557×10^{-9} $W^{-1}m^{-1}$, 5.601×10^{-9} $W^{-1}m^{-1}$, 5.623×10^{-9} $W^{-1}m^{-1}$ for RI of sensing analyte, n=1.35, 1.36, 1.37, 1.38, 1.39 respectively in Y polarized direction at 1.4THz frequency. Non-linearity values of 5.72×10^{-9} $W^{-1}m^{-1}$, 5.753×10^{-9} $W^{-1}m^{-1}$, 5.783×10^{-9} $W^{-1}m^{-1}$, 5.811×10^{-9} $W^{-1}m^{-1}$, 5.837×10^{-9} $W^{-1}m^{-1}$ were achieved for RI of sensing analyte n=1.35, 1.36, 1.37, 1.38, 1.39 respectively in X polarized direction at 1.4THz operating frequency.
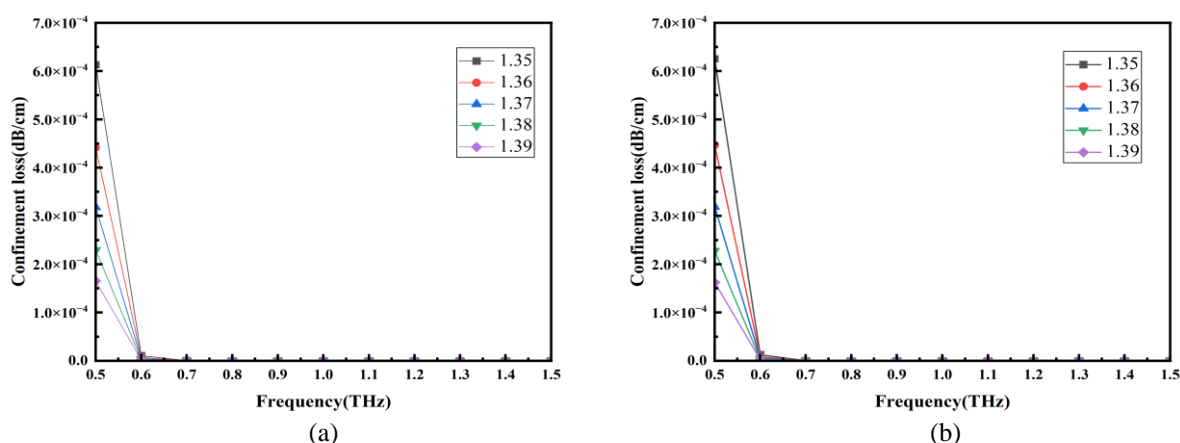

(a) (b)

Fig. 5.7 (a) and **(b)** Confinement Loss variation with frequency in X and Y polarization directions respectively

Fig. 5.7 (a,b) shows CL variation for both X and Y polarization directions in the 0.5-1.5 THz frequency range. The CL graph depicts that confinement loss decreases as frequency increases.

The confinement of lights gets better with larger frequencies as larger frequencies correspond to shorter wavelengths and shorter wavelengths are easier to confine within the fiber's periodic structure, the CL decreases for larger frequencies. Further with increase in frequency, the waveguide dispersion within the fiber becomes increasingly significant, which results in a more pronounced confinement of light within the core [24]. We observed the CL of 8.409×10^{-15} dB/cm, 8.659×10^{-15} dB/cm, 3.559×10^{-14} dB/cm, 3.849×10^{-14} dB/cm, 5.639×10^{-14} dB/cm for RI of analyte, n=1.35, 1.36, 1.37, 1.38, 1.39 respectively in Y polarized direction at 1.4 THz frequency. In X polarized direction we observed CL of 2.779×10^{-14} dB/cm, 2.489×10^{-16} dB/cm, 1.499×10^{-13} dB/cm, 7.479×10^{-14} dB/cm, 1.759×10^{-14} dB/cm for the RI of analyte, n=1.35, 1.36, 1.37, 1.38, 1.39 respectively at 1.4 THz frequency
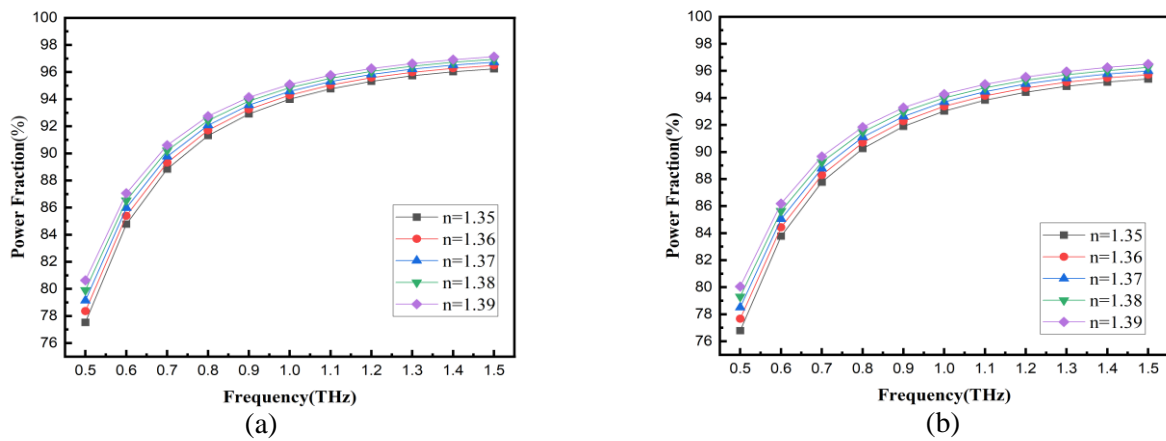

Fig. 5.8 (a) and **(b)** Power fraction variation with frequency in X and Y polarization directions respectively.

Fig. 5.8 (a, b) shows variation of power fraction of different analytes in X and Y polarized directions. One of the key factors influencing the sensor's performance is its sensitivity which is determined by Power fraction. The graph shows that core power fraction is generally more for analyte with higher refractive index. The values of power fraction have been achieved are 95.169%, 95.479%, 95.762%, 96.021%, 95.259% for RI of analyte n=1.35, 1.36, 1.37, 1.38, 1.39 respectively in Y polarized direction at 1.4THz frequency. We also observed power fraction values as 96.023%, 96.277%, 96.509%, 96.722%, 96.917% for RI of analyte n=1.35, 1.36, 137, 1.38, 1.39 respectively in X polarized direction at operating frequency of 1.4THz.

5.5 CONCLUSION

In this chapter, a rectangular core PCF sensor has been proposed for sensing different analyte with refractive index ranging from 1.35-1.39. The cladding is composed of rectangular shaped air holes. Zeonex is used as fiber material. The proposed refractive index fiber sensor can be

utilized for detection of many biological components such as blood components (RBC, WBC, Plasma etc.), various cancer cells etc. The proposed sensor shows a very high relative sensitivity of 98.8% and 98.035% for an analyte of refractive index 1.39 at 1.4 THz operating frequency in X and Y polarized direction respectively. Besides CL is noticed only 7.75×10^{-14} dB/cm and 5.627×10^{-14} dB/cm in X and Y polarized direction respectively for an analyte of refractive index 1.39. Furthermore, other optical properties such as effective refractive index, EMA, and Non-linearity have been achieved. It is possible to build the suggested PCF using the current fabrication techniques. The proposed model has demonstrated a preference for being satisfactory in detecting various analytes. The investigated PCF provides interesting findings and may find use in bio-sensing application.

CHAPTER-6

DESIGN AND ANALYSIS OF A RECTANGULAR CORE PHOTONIC CRYSTAL FIBER BIOSENSOR BASED ON TERAHERTZ REGIME FOR MALARIA DETECTION[1]

6.1 INTRODUCTION

Malaria is vector-borne diseases and a serious risk to human health worldwide especially in densely populated, under developed, tropical region. Malaria, a deadly disease caused by a parasite transmitted to humans through a particular species of mosquito that feed on human. Humans are infected by four distict kinds of malaria parasites namely Plasmodium falciparum, Plasmodium vivax, Plasmodium ovale, and Plasmodium malariae[45]. Malaria has three phases. The first cycle starts when the merozoites enter the red blood cells (RBCs) and transform into uni-nucleated trophozoites[46]. Trophozoites are transformed into schizonts, a kind of multinuclear cell, during the schizont phase. Early detection of malaria is very important and crucial for treating infected people and can lower mortality. Biosensors based on Photonic crystal fiber have a wide range of applications in biomedical explorations, biomolecule detection, and medical fields [47]. Change in refractive index is used to for identification of different stages of malaria. Various Traditional techniques are available for detection of malaria like clinical diagnosis which is based on symptoms and the physical health and signs of the patients, quantitative buffy coat (QBC)[45], polymerase chain reaction (PCR)-based technique, Loop-mediated isothermal amplification (LAMP)[48], flow cytometry (FCM)[49], automated blood cell counter (ACC), rapid diagnostic tests (RDTs), and mass spectrophotometry (MS) with the drawback that these techniques requires specialized devices, trained technicians, complex methodologies and are expensive. In contrast to this PCF sensors are highly sensitive, low cost, have straightforward detection technique, swift detection and offers remote diagnostics.

In this chapter we have introduced a Refractive index based highly sensitive PCF biosensor for detection of malaria at different stages in the intraerythrocytic cycle of plasmodium falciparum malaria. The distribution of RI is uniform in healthy RBCs and non-uniform in infected RBCs.

---

[1] A part of this chapter has been accepted for publication in ICAMNOP conference 2023, Springer Nature Proceeding

Table 1 shows the refractive index values of mlaria infected blood at different stages [45]. Consequently, there is a significant RI difference between infected and healthy RBCs. Therefore, one of the most important indicators for the diagnosis of malaria disorders is the RBCs refractive index. For background material zeonex is used which is a transparent thermoplastic. With the properties like low absorption loss of 0.2 cm^{-1}, high biocompatibility, low water absorption and optical characteristics like constant RI of 1.53 in THz regime therefore zeonex is preferred for biosensing applications[42].
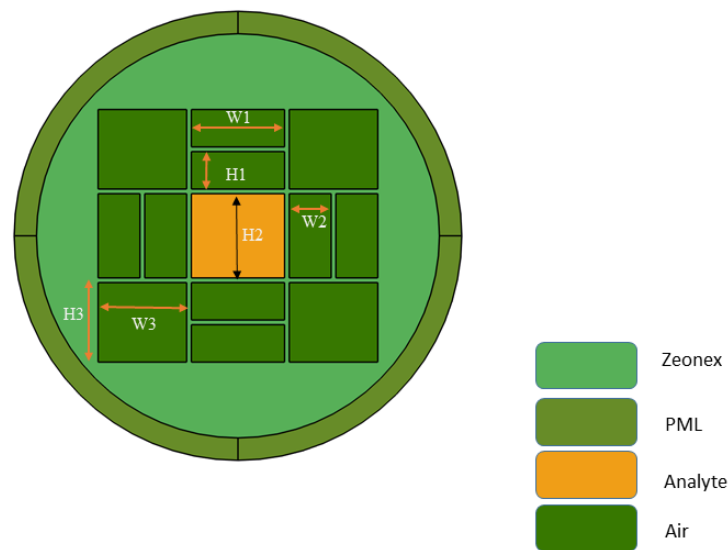

Fig. 6.1 Schematic cross-sectional view of the proposed biosensor

6.2 SENSOR MODEL DESIGN

The proposed PCF sensor has a hollow rectangular core and rectangular shaped air holes as demonstrated in Fig. 6.1. The radius of the proposed sensor is 1200 μm. Core dimensions are 450 μm height and 500 μm width. Other parameters include height H1, H2, H3 equal to 200 μm, 450 μm, 462.5 μm respectively and width W1, W2, W3 equal to 500 μm, 225 μm, 512.5 μm respectively. Two adjacent air holes are separate by a distance of 20μm. Complete mesh consists of 6650 domain elements and 866 boundary elements. To fabricate the PCF various techniques are there like stack and draw, extrusion, sol-gel, capillary stacking, and 3D printing. 3D printing and extrusion are suited for fabricating rectangular, square and elliptical air holes, which make sure that fabrication of proposed fiber is feasible. The hollow core is to be filled with RBC samples to detect malaria using selective filling method.
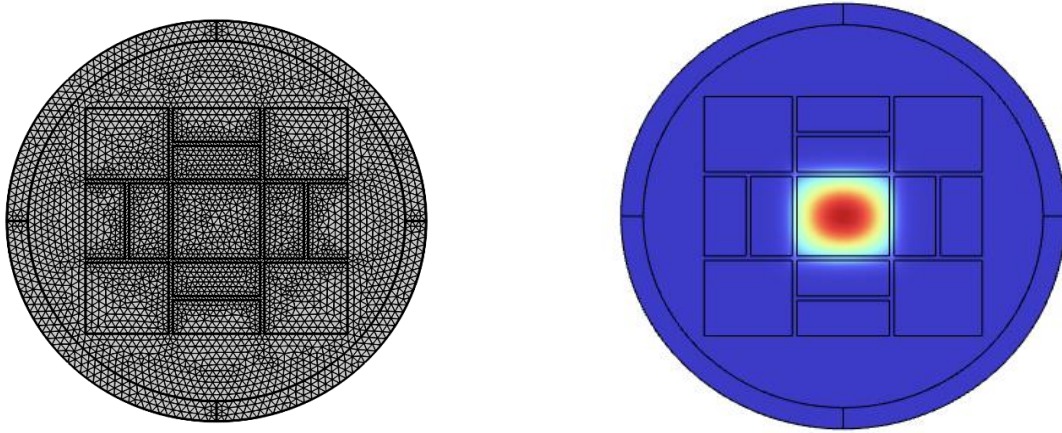
Fig. 6.2 (a) Mesh view of the proposed sensor (b) wave propagation profile of the proposed sensor

Stages	RI(n)
Normal RBCs	1.402
Malaria at Ring phase	1.395
Malaria at trophozoite phase	1.383
Malaria at schizont phase	1.373

Table 6.1. Malaria at different stages with respective refractive indices ate every stage

6.3 NUMERICAL ANALYSIS AND RESULTS

Numerical analysis is done in the similar way as done in previous chapter, hence in order to evaluate the potential of the proposed sensor various optical parameters are evaluated which include relative sensitivity, confinement loss (CL), effective mode index (n_{eff}), effective mode area (A_{eff}), and non-linearity(γ). After simulating the proposed design in COMSOL multiphysics software we got following results.

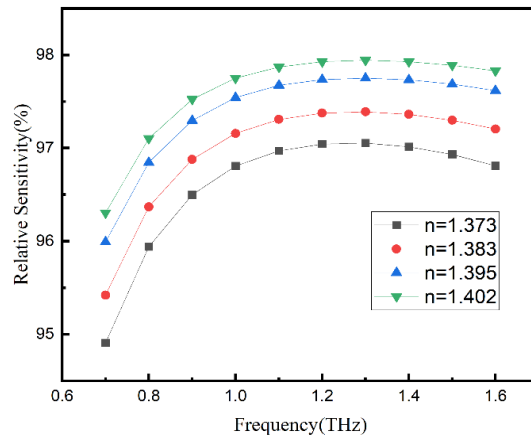Fig.6.3 Relative sensitivity variation with frequency

Fig. 6.3 shows relative sensitivity variation with frequency. Relative sensitivity increases as frequency increases and then slightly decreases. We achieved RS values of 97.942%, 97.75%, 97.389%, and 97.052% for normal RBCs, ring, trophozoite, and schizont phase respectively at 1.3THz operating frequency.
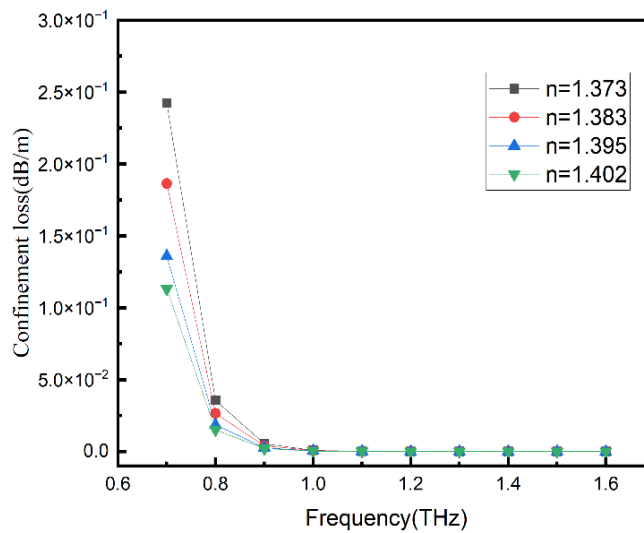

Fig.6.4 Confinement Loss variation with Frequency

Confinement loss is another important parameter and its variation with frequency is depicted by Fig. 6.4. CL values decreases as frequency increases this is because light confinement in the core increase with shorter wavelength, or high frequency as shorter the wavelength more will the confinement of light and dispersion becomes more prominent at higher frequencies , results in more confinement of light within the core . In this article we achieved CL values of 1.49×10^{-6} dB/m, 2.08×10^{-6} dB/m, 3.70×10^{-6} dB/m, 6.02×10^{-6} dB/m for normal RBCs, ring phase, trophozoite phase, and schizont phase malaria.
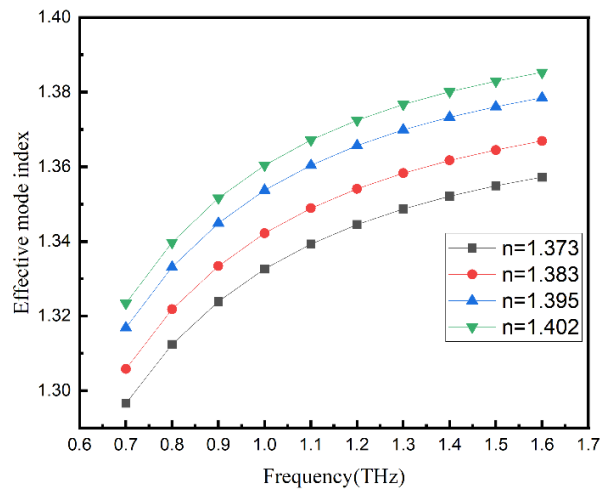
Fig. 6.5 Effective mode index versus frequency curve

Fig. 6.5 depicts the effective mode index of malaria at different stages with frequency. The values of EMI increases with increase in the frequency. The calculated values of n_{eff} that have been attained are 1.3767, 1.3699, 1.3583, 1.3487 for normal RBCs, ring, trophozoite, and schizont phase malaria at an operating frequency of 1.3THz.
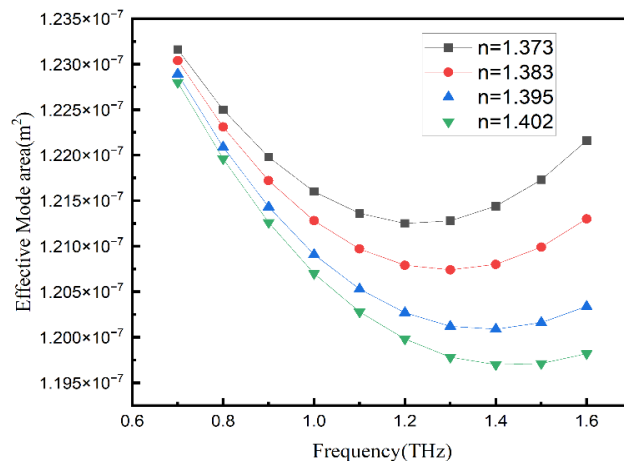

Fig.6.6 Effective mode area curve with frequency

33

Effective mode area is curve with frequency is shown by Fig. 6. With the variation of frequency from 0.7 THz to 1.6THz light is more confined in the core for larger values of the frequency. This confinement of light in core region results in lesser effective area. At 1.3THz frequency, the A_{eff} values obtained are 1.20×10^{-7} m^2, 1.20×10^{-7} m^2, 1.21×10^{-7} m^2, 1.21×10^{-7} m^2 for normal RBCs, ring phase, trophozoite phase, and schizont phase malaria at an operating frequency of 1.3THz.
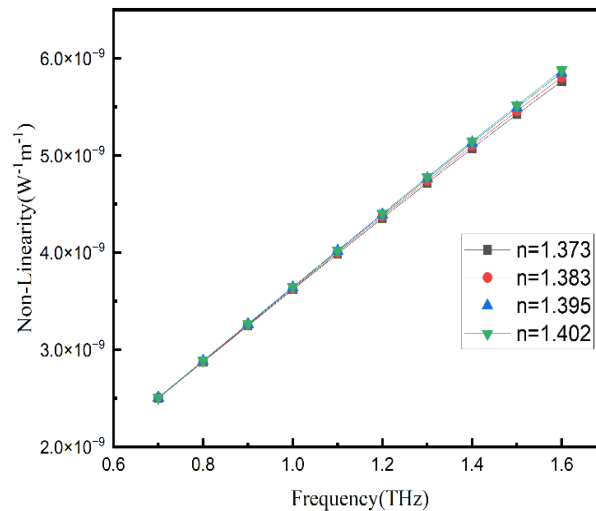

Fig 6.7. Non-linearity variation with respect to the frequency

Fig. 6.7 shows the Non-linearity fluctuation with frequency. Non-linearity changes linearly as the frequency increases. We achieved Non-linearity values of 4.78×10^{-9} W^{-1}m^{-1}, 4.76×10^{-9} W^{-1}m^{-1}, 4.74×10^{-9} W^{-1}m^{-1}, 4.72×10^{-9} W^{-1}m^{-1} for normal RBCs, ring phase, trophozoite phase, and schizont phase malaria at an operating frequency of 1.3THz.

6.4 CONCLUSION

A RI sensor based on terahertz regime for early detection of malaria is proposed with hollow rectangular core. The proposed sensor detects the change in RI of RBCs during various stages of malaria parasite in terahertz regime. Different sensor parameters such as Relative sensitivity, confinement loss, effective mode area, non-linearity and effective mode index are evaluated for different stages of malaria. With zeonex as fiber material rectangular hollow core is filled with infected RBCs for light-analyte interaction. Suggested fiber sensor remarkably high relative sensitivity of values of 97.942%, 97.75%, 97.389%, and 97.052% for normal RBC, ring phase, trophozoite phase, and schizont phase respectively at 1.3THz operating frequency. Table 2 compares the result of the previously proposed work with our work .With RS other

optical parameters are also determined which are confinement loss, effective area, non-linearity for evaluating the potential of proposed fiber sensor.

Ref.	Detection target	Operating frequency	Background material	Effective Mode Area	Relative Sensitivity	Confinement Loss
[42]	Blood Components(RBCs, hemoglobin, WBCs, Plasma, water)	1.5THz	Topas	1.55×10^5 μm^2	80.93%, 80.56%, 80.13%, 79.91% 79.39%	1.23×10^{-12} dB/m, 8.63×10^{-12} dB/m, 4.93×10^{-12} dB/m, 2.93×10^{-12} dB/m 1.13×10^{-12} dB/m
[51]	Chemical (Ethanol, Benzene, Water)	1THz	Silica	1.6285×10^{-7} m^2	68.48%, 69.20%, 66.78%	2.13×10^{-9} dB/m ,1.92×10^{-9} dB/m, 2.70×10^{-6} dB/m
[52]	Biosensor(Tuberculosis)	2.2 THz	Zeonex	0.15×10^{-8} m^2	90.60%	3.13×10^{-9} cm^{-1}
This work	Malaria	1.3 THz	Zeonex	1.20×10^{-7} m^2, 1.20×10^{-7} m^2, 1.21×10^{-7} m^2, 1.21×10^{-7} m^2	97.942%, 97.75%, 97.389%, 97.052%	1.49×10^{-6} dB/m, 2.08×10^{-6} dB/m, 3.70×10^{-6} dB/m, 6.02×10^{-6} dB/m

Table 6.2 Comparison of results of previously proposed refractive index sensor and our work

CHAPTER-7

CONCLUSION AND SCOPE FOR FUTURE WORK

7.1 Conclusion

In this work, we have demonstrated Photonic Crystal Fiber based terahertz sensor for biochemical sensing application. The proposed sensors are refractive index sensors which are sensitive to change in refractive index of the analyte. Rectangular core photonic crystal fibers with zeonex as a background material has been proposed which can be used to detect various cancer cells, blood components, malaria at different stages. All the proposed design are simulated and numerically analyzed in COMSOL Multiphysics software. Various optical parameters, like relative sensitivity, confinement loss, effective mode area, non-linearity, birefringence, are evaluated for the performance analysis of the fiber. We achieved a very high sensitivity of 98.8% for an analyte of refractive index 1.39 at 1.4 THz operating frequency and low confinement loss of order 10^{-14} dB/cm. Various fabrication processes are also suggested. The proposed models has shown a commendable level of efficacy in detecting a variety of analytes. The examined photonic crystal fiber (PCF) yields intriguing results, indicating its potential utility in bio-sensing applications.

7.2 Future Works and Scope

Photonic Crystal fiber shows a great potential as sensors because of their various advantages and properties. This work can further be extended

1. To develop and model more sensitive and fabrication-friendly designs that are more feasible for practical applications.

2. To design and develop Surface Plasmon Resonance based terahertz sensors which are very sensitive to refractive index variation.

3. Further machine learning algorithms can be incorporated with present optical fiber technology in order to increase the sensitivity of the fiber sensors, overall increasing the practicality so that fiber sensors can be used in real world applications.

LIST OF PUBLICATIONS

Article in Refereed International Journal (Thesis)

1. Singh, N., Khamaru, A. & Kumar, A. Design and analysis of a rectangular core refractive index-based PCF sensor for bio-sensing application. *Opt Quant Electron* **56**, 1133 (2024). https://doi.org/10.1007/s11082-024-07076-1

Articles in Conference Preceedings (Thesis)

1. "Design And Analysis of a Rectangular Core Photonic Crystal Fiber Biosensor Based on Terahertz Regime for Malaria Detection" (Accepted ICAMNOP springer nature proceedings)

REFERENCES

[1] Ghatak, A. K., & Thyagarajan, K. (1998). *An introduction to fiber optics*. Cambridge university press.

[2] Kao, K. C., & Hockham, G. A. (1966, July). Dielectric-fibre surface waveguides for optical frequencies. In *Proceedings of the Institution of Electrical Engineers* (Vol. 113, No. 7, pp. 1151-1158). IET Digital Library.

[3]Addanki, S., Amiri, I. S., & Yupapin, P. (2018). Review of optical fibers-introduction and applications in fiber lasers. *Results in Physics*, *10*, 743-750.

[4] Hanover, M. D. (2021). A Brief Introduction to Core Modes in Optical Fiber.

[5] Okoshi, T. (2012). *Optical fibers*. Elsevier.

[6] Ainslie, B., & Day, C. (1986). A review of single-mode fibers with modified dispersion characteristics. *Journal of lightwave technology*, *4*(8), 967-979.

[7] Poli, F., Cucinotta, A., & Selleri, S. (2007). *Photonic crystal fibers: properties and applications* (Vol. 102). Springer Science & Business Media.

[8] Haakestad, M.W., & Engan, H.E. (2006). Acoustooptic properties of a weakly multimode solid core photonic crystal fiber. *Journal of Lightwave Technology, 24*, 838-845.

[9] Cregan, R. F., Mangan, B. J., Knight, J. C., Birks, T. A., Russell, P. S. J., Roberts, P. J., & Allan, D. C. (1999). Single-mode photonic band gap guidance of light in air. *science*, *285*(5433), 1537-1539.

[10] Reyes-Vera, E., Usuga-Restrepo, J., Jimenez-Durango, C., Montoya-Cardona, J., & Gomez-Cardona, N. (2018). Design of low-loss and highly birefringent porous-core photonic crystal fiber and its application to terahertz polarization beam splitter. *IEEE Photonics Journal*, *10*(4), 1-13.

[11] Benabid, F., & Roberts, P. J. (2011). Linear and nonlinear optical properties of hollow core photonic crystal fiber. *Journal of Modern Optics*, *58*(2), 87-124.

[12] Benabid, F., Knight, J. C., Antonopoulos, G., & Russell, P. S. J. (2002). Stimulated Raman scattering in hydrogen-filled hollow-core photonic crystal fiber. *Science*, *298*(5592), 399-402.

[13] Couny, F., Benabid, F., Roberts, P. J., Light, P. S., & Raymer, M. G. (2007). Generation and photonic guidance of multi-octave optical-frequency combs. *Science*, *318*(5853), 1118-1121.

[14] Bao, H., Nielsen, K., Rasmussen, H. K., Jepsen, P. U., & Bang, O. (2012). Fabrication and characterization of porous-core honeycomb bandgap THz fibers. *Optics express*, *20*(28), 29507-29517.

[15] Bise, R. T., & Trevor, D. J. (2005, March). Sol-gel derived microstructured fiber: fabrication and characterization. In *Optical Fiber Communication Conference* (Vol. 3, p. 3). Anaheim, CA, USA: Optical Society of America.

[16] Ghazanfari, A., Li, W., Leu, M. C., & Hilmas, G. E. (2017). A novel freeform extrusion fabrication process for producing solid ceramic components with uniform layered radiation drying. *Additive Manufacturing*, *15*, 102-112.

[17] Ebendorff-Heidepriem, H., Schuppich, J., Dowler, A., Lima-Marques, L., & Monro, T. M. (2014). 3D-printed extrusion dies: a versatile approach to optical material processing. *Optical Materials Express*, *4*(8), 1494-1504.

[18] BASAK, R. K. (2018). *Development of specialty photonic crystal fiber for plasmonic applications* (Doctoral dissertation, CSIR-Central Glass and Ceramic Research Institute).

[19] Panda, A., & Pukhrambam, P. D. (2021). Design and analysis of porous core photonic crystal fiber based ethylene glycol sensor operated at infrared wavelengths. *Journal of computational electronics*, *20*, 943-957.

[20] Arif, M. F. H., Ahmed, K., Asaduzzaman, S., & Azad, M. A. K. (2016). Design and optimization of photonic crystal fiber for liquid sensing applications. *Photonic Sensors*, *6*, 279-288.

[21] Xu, H., Wang, X., Kong, Q., & Peng, D. (2020). High numerical aperture photonic crystal fiber with silicon nanocrystals core for optical coherence tomography. *Optik*, *219*, 165000.

[22] Sen, S., Abdullah-Al-Shafi, M., Sikder, A. S., Hossain, M. S., & Azad, M. M. (2021). Zeonex based decagonal photonic crystal fiber (D-PCF) in the terahertz (THz) band for chemical sensing applications. *Sensing and Bio-Sensing Research*, *31*, 100393.

[23] Islam, M. R., Iftekher, A. N. M., Mou, F. A., Rahman, M. M., & Bhuiyan, M. I. H. (2021). Design of a Topas-based ultrahigh-sensitive PCF biosensor for blood component detection. *Applied Physics A*, *127*, 1-16.

[24] Yadav, S., Lohia, P., Dwivedi, D.K.: A novel approach for identification of cancer cells using a photonic crystal fiber-based sensor in the terahertz regime. Plasmonics 18, 1753–1769 (2023).

[25] Finazzi, V., Monro, T. M., & Richardson, D. J. (2003). Small-core silica holey fibers: nonlinearity and confinement loss trade-offs. *JOSA B*, *20*(7), 1427-1436.

[26] Habib, M.A., Anower, M.S., Abdulrazak, L.F., Reza, M.S.: Hollow core photonic crystal fiber for chemi cal identification in terahertz regime. Opt. Fiber Technol. (2019). https://doi.org/10.1016/j.yofte.2019. 101933

[27] Almawgani, A. H., Alhamss, D. N., Taya, S. A., Hindi, A. T., Upadhyay, A., Singh, S., ... & Patel, S. K. (2023). Theoretical analysis of a refractive index sensor based on a photonic crystal fiber with a rectangular core. *Optical and Quantum Electronics*, *55*(10), 881.

[28] Zhang, T., Zheng, Y., Wang, C., Mu, Z., Liu, Y., & Lin, J. (2018). A review of photonic crystal fiber sensor applications for different physical quantities. *Applied Spectroscopy Reviews*, *53*(6), 486-502.

[29] Islam, M. S., Sultana, J., Rifat, A. A., Dinovitser, A., Ng, B. W. H., & Abbott, D. (2018). Terahertz sensing in a hollow core photonic crystal fiber. *IEEE Sensors Journal*, *18*(10), 4073-4080.

[30] Islam, M. R., Khan, M. M. I., Mehjabin, F., Chowdhury, J. A., & Islam, M. (2020). Design of a fabrication friendly & highly sensitive surface plasmon resonance-based photonic crystal fiber biosensor. *Results in Physics*, *19*, 103501.

[31] Ramani, U., Kumar, H., Kumar, R., Singh, B. K., & Pandey, P. C. (2023). Rectangular-shape cladding-based photonic crystal fiber surface plasmon resonance-based refractive index sensor. *Plasmonics*, *18*(3), 921-929.

[32] Ramola, A., Marwaha, A., & Singh, S. (2021). Design and investigation of a dedicated PCF SPR biosensor for CANCER exposure employing external sensing. *Applied Physics A*, *127*(9), 643.

[33] Dong, X., Du, H., Sun, X., Luo, Z., & Duan, J. A. (2018). A novel strain sensor with large measurement range based on all fiber Mach-Zehnder interferometer. *Sensors*, *18*(5), 1549.

[34] Hou, M., Wang, Y., Liu, S., Li, Z., & Lu, P. (2016). Multi-components interferometer based on partially filled dual-core photonic crystal fiber for temperature and strain sensing. *IEEE Sensors Journal*, *16*(16), 6192-6196.

[35] Naeem, K., Kwon, I. B., & Chung, Y. (2017). Multibeam interferometer using a photonic crystal fiber with two asymmetric cores for torsion, strain and temperature sensing. *Sensors*, *17*(1), 132.

[36] Sultana J, Islam MdS, Ahmed K, et al (2018) Terahertz detection of alcohol using a photonic crystal fiber sensor. Appl Opt 57:2426. https://doi.org/10.1364/ao.57.002426

[37] El Haddad J, Bousquet B, Canioni L, Mounaix P (2013) Review in terahertz spectral analysis. TrAC - Trends in Analytical Chemistry 44:98–105

[38] Ekhlasur Rahaman M, Bellal Hossain M, Shekhar Mondal H, et al (2020) Highly sensitive photonic crystal fiber liquid sensor in terahertz frequency range. In: Materials Today: Proceedings. Elsevier Ltd, pp 3815–3820

[39] Hossain MB, Podder E (2019) Design and investigation of PCF-based blood components sensor in terahertz regime. Appl Phys A Mater Sci Process 125:. https://doi.org/10.1007/s00339-019-3164-x

[40] Selim Hossain M, Sen S Design and Performance Improvement of Optical Chemical Sensor Based Photonic Crystal Fiber (PCF) in the Terahertz (THz) Wave Propagation. https://doi.org/10.1007/s12633-020-00696-8/Published

[41] Rahaman ME, Jibon RH, Mondal HS, et al (2021) Design and optimization of a PCF-based chemical sensor in THz regime. Sens Biosensing Res 32:. https://doi.org/10.1016/j.sbsr.2021.100422

[42] Ahmed K, Ahmed F, Roy S, et al (2019) Refractive Index-Based Blood Components Sensing in Terahertz Spectrum. IEEE Sens J 19:3368–3375. https://doi.org/10.1109/JSEN.2019.2895166

[43] Bulbul AAM, Kouzani AZ, Mahmud MAP, Nahid A Al (2021) Design and Numerical Analysis of a Novel Rectangular PCF (R-PCF)-Based Biochemical Sensor (BCS) in the THz Regime. Int J Opt 2021:. https://doi.org/10.1155/2021/5527724

[44] Bulbul AAM, Rahaman H, Podder E (2022) Design and quantitative analysis of low loss and extremely sensitive PCF-based biosensor for cancerous cell detection. Opt Quantum Electron 54:. https://doi.org/10.1007/s11082-022-03513-1.

[45] V. S. Chaudhary, D. Kumar, and S. Kumar, "Gold-Immobilized Photonic Crystal Fiber-Based SPR Biosensor for Detection of Malaria Disease in Human Body," *IEEE Sens J*, vol. 21, no. 16, pp. 17800–17807, Aug. 2021, doi: 10.1109/JSEN.2021.3085829.

[46] K. V. Ragavan, S. Kumar, S. Swaraj, and S. Neethirajan, "Advances in biosensors and optical assays for diagnosis and detection of malaria," *Biosensors and Bioelectronics*, vol. 105. Elsevier Ltd, pp. 188–210, May 15, 2018. doi: 10.1016/j.bios.2018.01.037.

[47] N. A. N. Binti Suhaimi, I. K. Yakasai, E. Abas, S. Kaijage, and F. Begum, "Modelling and simulation of novel liquid-infiltrated PCF biosensor in Terahertz frequencies," *IET Optoelectronics*, vol. 14, no. 6, pp. 411–416, Dec. 2020, doi: 10.1049/iet-opt.2020.0069.

[48] P. Deng, S. P. Zhao, H. Y. Dai, X. S. Guan, and H. G. Huang, "Atorvastatin reduces the expression of COX-2 mRNA in peripheral blood monocytes from patients with acute myocardial infarction and modulates the early inflammatory response," *Clin Chem*, vol. 52, no. 2, pp. 300–303, Feb. 2006, doi: 10.1373/clinchem.2005.057893.

[49] Wongchotigul, V., Suwanna, N., Krudsood, S., Chindanond, D., Kano, S., Hanaoka, N., Akai, Y., Maekawa, Y., Nakayama, S., Kojima, S. and Looareesuwan, S., 2004. The use of flow cytometry as a diagnostic test for malaria parasites. *Southeast Asian journal of tropical medicine and public health*, *35*, pp.552-559.

[50] M. Selim Hossain and S. Sen, "Design and Performance Improvement of Optical Chemical Sensor Based Photonic Crystal Fiber (PCF) in the Terahertz (THz) Wave Propagation", doi: 10.1007/s12633-020-00696-8/Published.

[51] N. A. Mohammed, O. E. Khedr, E. S. M. El-Rabaie, and A. A. M. Khalaf, "High-Sensitivity Early Detection Biomedical Sensor for Tuberculosis With Low Losses in the Terahertz Regime Based on Photonic Crystal Fiber Technology," *Photonic Sensors*, vol. 13, no. 2, Jun. 2023, doi: 10.1007/s13320-023-0675-z.

APPENDIX 1: PLAGARISM REPORT

PAPER NAME

Thesis (4)-pages-deleted.pdf

AUTHOR

NEERAJ SINGH

WORD COUNT

12123 Words

CHARACTER COUNT

69644 Characters

PAGE COUNT

51 Pages

FILE SIZE

2.7MB

SUBMISSION DATE

Jun 6, 2024 12:40 PM GMT+5:30
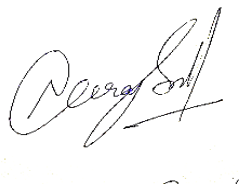
REPORT DATE

Jun 6, 2024 12:41 PM GMT+5:30

● 9% Overall Similarity

The combined total of all matches, including overlapping sources, for each database.

- 5% Internet database
- 7% Publications database
- Crossref database
- Crossref Posted Content database
- 3% Submitted Works database

● Excluded from Similarity Report

- Bibliographic material
- Quoted material
- Cited material
- Small Matches (Less then 12 words)
- Manually excluded sources

44

9 Teaching and Learning with Technology on 2023-10-26
Submitted works
<1%

10 Qing Chen, Jingzhi Wu, Yanhong Wang, Mengwei Li. "Terahertz Anti-re...
Crossref
<1%

11 digibuo.uniovi.es
Internet
<1%

12 diva-portal.org
Internet
<1%

13 d-scholarship.pitt.edu
Internet
<1%

14 University of Asia Pacific on 2021-06-05
Submitted works
<1%

15 journals.riverpublishers.com
Internet
<1%

16 S.K. Sarkar, A.K. Nayak, K.V.S. RamaRao, J.P. Mittal. "Isotope selective...
Crossref
<1%

17 Sultan Qaboos University on 2024-04-20
Submitted works
<1%

18 E. Cisneros, J.H. Caltenco, R.M. Linares. "Cylindrical Transmission Line...
Crossref
<1%

19 Gokten, Mesut. "New frequency domain electromagnetic solvers based...
Publication
<1%

20 Md. Ekhlasur Rahaman, Rayhan Habib Jibon, Himadri Shekhar Mondal,...
Crossref
<1%

21 Satish Addanki, I.S. Amiri, P. Yupapin. "Review of optical fibers-introdu... <1%
    Crossref

22 Universiti Teknologi MARA on 2016-01-04 <1%
    Submitted works

23 Baljinder Kaur, Santosh Kumar, Brajesh Kumar Kaushik. "Advances in p... <1%
    Crossref

24 Universiti Brunei Darussalam on 2022-04-26 <1%
    Submitted works

25 Xiao, Limin. "Novel splice techniques and micro-hole collapse effect in ... <1%
    Publication

26 en.wikipedia.org <1%
    Internet

27 Abdulkarem H. M. Almawgani, Dana N. Alhamss, Sofyan A. Taya, Aym... <1%
    Crossref

28 Birla Institute of Technology and Science Pilani on 2021-03-13 <1%
    Submitted works

29 Hao Chang, Yichao Meng. "Terahertz polymer vortex photonic crystal fi... <1%
    Crossref

30 Indian Institute of Technology Patna on 2016-04-23 <1%
    Submitted works

31 Malaviya National Institute of Technology on 2011-05-05 <1%
    Submitted works

32 Md. Saiful Islam, Jakeya Sultana, Mohammad Faisal, Mohammad Raki... <1%
    Crossref

45	ir.nctu.edu.tw Internet	<1%
46	mdpi-res.com Internet	<1%
47	old.spuvvn.edu Internet	<1%
48	publications.polymtl.ca Internet	<1%

● **Excluded from Similarity Report**

- Bibliographic material
- Cited material
- Manually excluded sources
- Quoted material
- Small Matches (Less then 12 words)

EXCLUDED SOURCES

| link.springer.com
Internet | 22% |
| Neeraj Singh, Akash Khamaru, Ajeet Kumar. "Design and analysis of a rectang...
Crossref | 22% |

NOTE- Excluded work is the published work which is the outcome of this thesis.

APPENDIX 2: PAPER ACCEPTANCE MAIL

Optical and Quantum Electronics: Decision on "Design and Analysis of a Rectangular Core Refractive Index- based PCF Sensor for Bio-sensing Application" Inbox

Optical and Quantum Electronics <do-not-reply@springernature.com>   Sat, May 11, 11:12 AM
to me

Dear Dr singh,

Re: "Design and Analysis of a Rectangular Core Refractive Index- based PCF Sensor for Bio-sensing Application"

We are delighted to let you know that the above submission, which you co-authored, has been accepted for publication in Optical and Quantum Electronics.

Please contact the corresponding author if you would like further details on this decision, including any reviewer feedback.

Thank you for choosing Optical and Quantum Electronics and we look forward to publishing your article.

Kind regards,

Editorial Assistant
Optical and Quantum Electronics

This message has been sent by the EquinOCS system
https://equinocs.springernature.com/

PLEASE DO NOT REPLY

========

Dear AJEET KUMAR,

We are pleased to inform you that your paper

037: "Design and analysis of a Rectangular Core Photonic Crystal Fiber biosensor based on Terahertz regime for Malaria Detection"
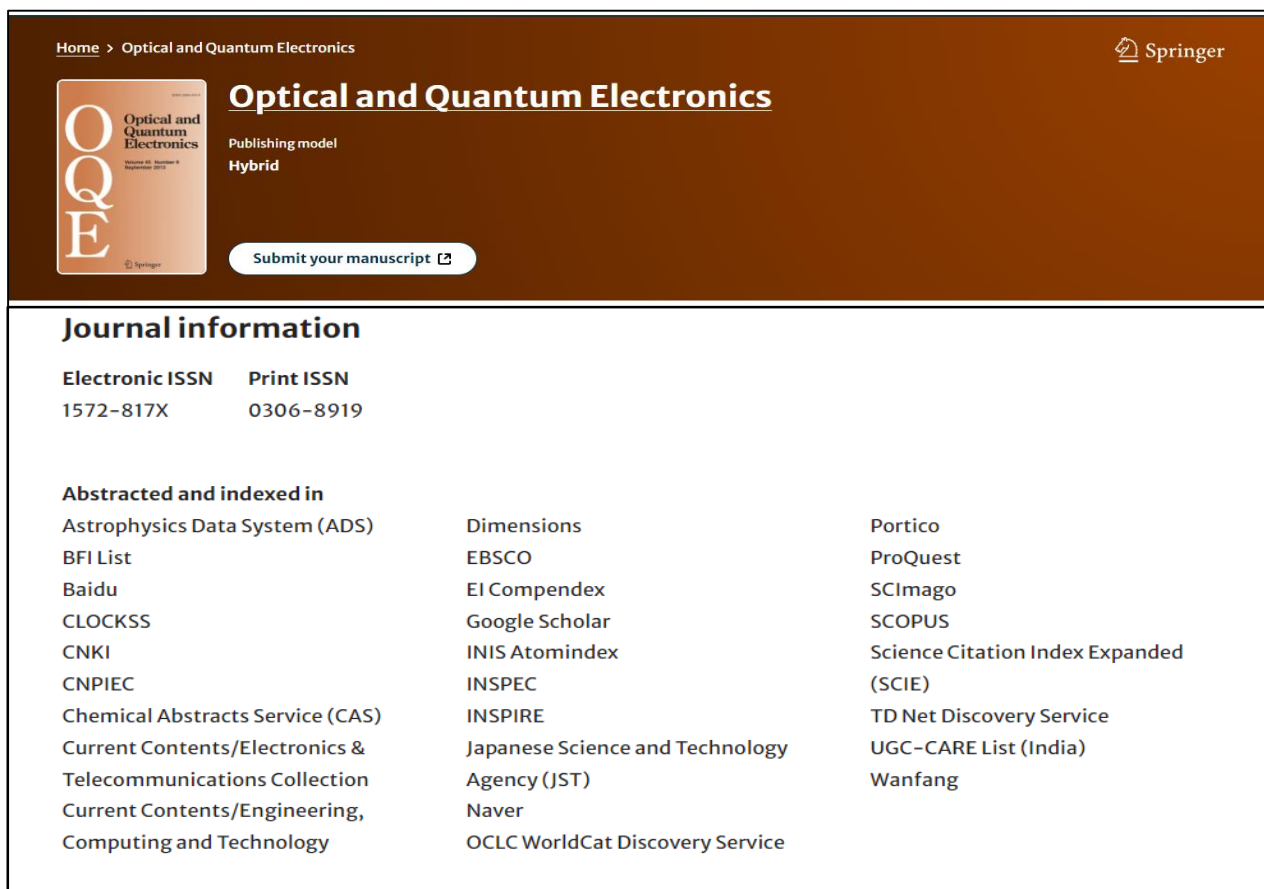
has been accepted for

International Conference on Atomic, Molecular, Material, Nano, and Optical Physics with Applications (ICAMNOP-2023)

Please find the reports beneath.

APPENDIX 3: PROOF OF SCOPUS/SCI INDEX

1. Optical and Quantum Electronics

Home > Optical and Quantum Electronics

Springer

Optical and Quantum Electronics

Publishing model
Hybrid

Submit your manuscript

Journal information

Electronic ISSN   **Print ISSN**
1572-817X   0306-8919

Abstracted and indexed in

Astrophysics Data System (ADS)	Dimensions	Portico
BFI List	EBSCO	ProQuest
Baidu	EI Compendex	SCImago
CLOCKSS	Google Scholar	SCOPUS
CNKI	INIS Atomindex	Science Citation Index Expanded
CNPIEC	INSPEC	(SCIE)
Chemical Abstracts Service (CAS)	INSPIRE	TD Net Discovery Service
Current Contents/Electronics &	Japanese Science and Technology	UGC-CARE List (India)
Telecommunications Collection	Agency (JST)	Wanfang
Current Contents/Engineering,	Naver	
Computing and Technology	OCLC WorldCat Discovery Service	

2. Springer's Proceeding in Physics

International Conference on Atomic, Molecular, Material, Nano and Optical Physics with Applications (ICAMNOP–2023)
Organized by: Department of Applied Physics, Delhi Technological University Delhi-110042, India
December 20th-22nd, 2023

HOME   CONFERENCE   COMMITTEE   SPEAKERS   PUBLICATION   REGISTRATION   ABSTRACTS   ACCOMMODATION   TOUR   GALLERY   CONTACT US

Login

Publication

The papers will be published in the Scopus indexed Springer's Proceedings in Physics (https://www.springer.com/series/361) after peer review.

Proceedings of our last International conference CAMNP 2019 was also published in Scopus indexed Springer's Proceedings in Physics https://link.springer.com/book/10.1007/978-981-16-7691-8

Springer Proceedings in Physics 271

Vinod Singh · Rinku Sharma ·
Man Mohan · Mohan Singh Mehata ·
A. K. Razdan *Editors*

Proceedings
of the International

APPENDIX 4: PUBLISHED WORK

Check for updates

Design and analysis of a rectangular core refractive index-based PCF sensor for bio-sensing application

Neeraj Singh[1] · Akash Khamaru[1] · Ajeet Kumar[1]

Abstract

A hollow-core photonic crystal fiber based Refractive Index sensor in the terahertz frequency regime for bio-sensing application is proposed in this paper. Refractive index variation is used for the identification of different analytes with refractive indices ranging from n = 1.35 to 1.39. Zeonex is chosen as the fiber material. The proposed photonic crystal fiber (PCF) sensor features a solitary rectangular core enclosed by an arrangement of 16 rectangular air holes within the cladding area with different heights and widths. Simulation and numerical analysis are conducted using Finite Element Method-based based Comsol Multiphysics Software. The proposed PCF sensor exhibits relative sensitivity of 98.8%, an Effective Mode Area of 1.06×10^{-7} m^2 with a very low confinement loss of 7.751×10^{-14} dB/cm are achieved at a frequency of 1.4 THz for an analyte of refractive index 1.39 in X Polarization direction of electric field. Moreover, birefringence, non-linearity, effective refractive index and power fraction are also analyzed. Further simple PCF structure based on rectangle ensures that fabrication is feasible with current fabrication techniques.

Keywords Terahertz frequency regime · Rectangular core · Relative sensitivity · Biosensor

1 Introduction

Photonic crystal fibers are attracting attention in the terahertz (THz) range for their unique capabilities in guiding and manipulating electromagnetic waves. Moreover, high sensitivity, compact size, low cost, flexibility, and fast response make them ideal for a variety of sensing applications (Sultana et al. 2018). Particularly, bio-chemical sensing which includes detecting or sensing of various biological components such as different types of cancer cells, blood components, analysis of RNA, DNA, and proteins and malaria cells. Utilizing the low photon energy within the THz range, THz sensors offer exceptional penetration capability through porous samples while maintaining test layer integrity (Haddad et al. 2013). Furthermore, PCFs operating in the THz range offer

---

✉ Ajeet Kumar
ajeetdph@dtu.ac.in

[1] Advanced Photonics Simulation Research Laboratory, Department of Applied Physics, Delhi Technological University, Delhi, India

significant advantages in terms of sensing analyte due to their large filling area, as the diameter of air holes and fiber diameter is larger than PCFs that are being operated in the mid-infrared range (Ekhlasur Rahaman et al. 2020). Due to these properties, various THz sensors and detectors have been developed using PCF. The hexagonal, octagonal, elliptical, rectangular structure of photonic crystal fiber has already been introduced, with a hollow core or solid core. Hollow core fibers offer higher sensitivity than solid core fibers. Hollow-core fibers (HCFs) exhibit superior suitability for detecting distinct analytes having lower RI and also offer strong light-analyte interaction within the core (Hossain and Podder 2019). Compared to solid core or porous core PCF, HC-PCF has a larger core power fraction and a lower effective material loss since the core is only filled with the target analyte.

PCF is becoming an increasingly important component of contemporary biological and biomedical technology since it may be used to detect blood components and cancer cells in both invasive and non-invasive ways among other things. The traditional techniques, which are employed for various pathological examinations and imaging, take a very long time to perform and obtain findings. The terahertz radiation band has garnered significant attention from the scientific community in recent times as it is possible to transmit terahertz radiation using PCFs without any risk to human health (Ferdous et al. 2022). Numerous THz optical sensors have been documented for use in biological applications. The advantages of PCF enable researchers to test different models for the detection of different analytes. Arif et el. proposed a chemical sensor, having a hexagonal cladding with circular air holes for liquid sensing and attained a relative sensitivity value of 50%, 55.83%, and 59.07% for water, ethanol, and benzene, respectively (Arif et al. 2016). A PCF sensor based on terahertz regime suggested by Islam et al. achieved a relative sensitivity of 68.87% for Ethanol (Islam et al. 2018). A chemical sensor with rotated hexacore and heptagonal cladding design with circular holes proposed by Selim Hossain et al. exhibit a relative sensitivity of 68.48%, 69.20%, 66.78% for ethanol, benzene, and water analyte at 1 THz (Selim Hossain and Sen 2021). Rahaman et al. suggested a dumbbell shaped HC-PCF with rectangular air holes for chemical sensing using TOPAS as the fiber material and achieved a relative sensitivity of 96.25% for Ethanol (Rahaman et al. 2021). Hossain et al. investigated a rectangular core sensor for Bane chemical detection and achieved a relative sensitivity of 94.4% and a confinement loss of 1.71×10^{-14} cm^{-1} at frequency 1.8 THz (Hossain et al. 2020). Ahmed et al. proposed a blood component sensor for analytes such as RBCs, hemoglobin, WBCs, plasma, and water and achieved a sensitivity response of 80.93%, 80.56%, 80.13%, 79.91% and 79.39% at frequency 1.5 THz (Ahmed et al. 2019). Bulbul et al. investigated a general purpose biochemical sensor with rectangular air holes and obtained a relative sensitivity of 95.82% at 2.5 THz (Bulbul et al. 2021).

The proposed sensor is a refractive index sensor which means the difference in refractive index is used for the identification of different analytes with RI ranging from 1.35 to 1.39. Zeonex is used as the background material. Zeonex is a transparent thermoplastic. It is preferred due to its wide range of optical characteristics, including its consistent refractive index of 1.53 in the THz regime, low absorption loss of 0.2 cm^{-1}, high glass transition temperature, minimal water absorption, high biocompatibility, and exceptional chemical resistance even at high temperatures (Yadav et al. 2023). Rectangular air holes are introduced in the fiber with a rectangular hollow core in which analytes are filled. A full vector FEM is used for numerical analysis and COMSOL multiphysics software is used for simulation.

2 Sensor model design

Figure 1 displays the cross-sectional representation of the proposed PCF sensor. Zeonex is used as background materials with rectangular air holes and a rectangular core. The rectangular air holes of different widths and heights are arranged across PCF. The overall diameter of the proposed diameter is 3.3 mm. The Perfectly matched layer (PML) occupies the cladding area and serves as an artificial absorbing medium to absorb radiation energy at the outer surface in the computational area and the width of the PML is 165 µm. Within the domain, the complete mesh consists of 24,554 elements while along the boundary it comprises 2452 elements. The width W1 and height H1 of the core is 400 µm and 500 µm respectively. Width W2 is 200 µm and H2 is 1540 µm respectively. Parameters W3 and W4 are 1720 µm and 1520 µm respectively. Parameters H2, H3, H4 are 1540 µm, 1340 µm, 1240 µm respectively. The pitch (separation between two adjacent rectangles) is 20 µm. The core is infiltrated with analyte samples with refractive index ranges from 1.35 to 1.39 serving as a region where light analyte interaction takes place. To begin the study, firstly the core of the PCF sensor is injected with the liquid analyte. Figure 2 shows the light propagation through the core filled with analyte. Since very little light leaves the core region, there is very little loss. The red region exhibits the highest degree of light confinement, and as it approaches the core boundary, the light's intensity progressively drops which shows light well confined in core region. Furthermore, the direction of electric and magnetic field is shown by arrow. To measure the efficacy of the proposed sensor, vivid sensing properties such as relative senitivity, birefringence, effective mode area, and confinement loss are used as measures.

3 Fabrication feasibility

Various techniques like stack and draw (Bao et al. 2010), drilling, extrusion (Ghazanfari et al. 2017), sol–gel (Bise and Trevor 2005), capillary stacking, and 3D printing (Ebendorff-Heidepriem et al. 2014) are available for the fabrication of Photonic Crystal Fibers. The capillary stacking, stack and draw, and sol–gel fabrication techniques are ideal for circular-shaped air hole fabrication. Alternatively, asymmetrical PCF designs with
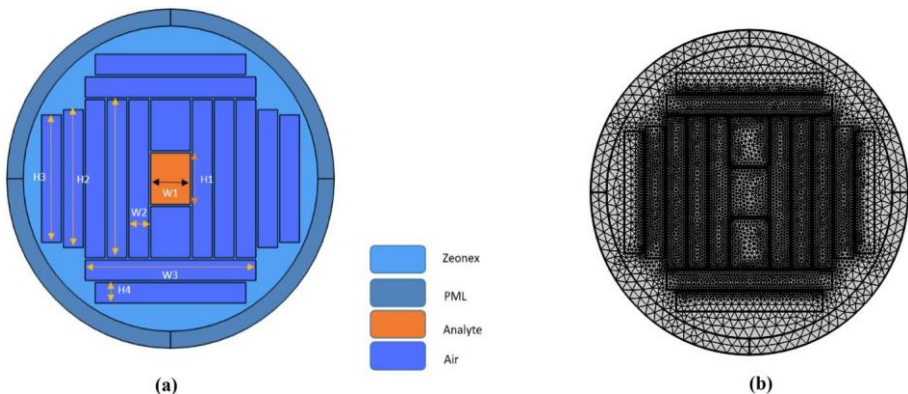

Fig. 1 **a** and **b** Sensor model design and meshing of proposed sensor
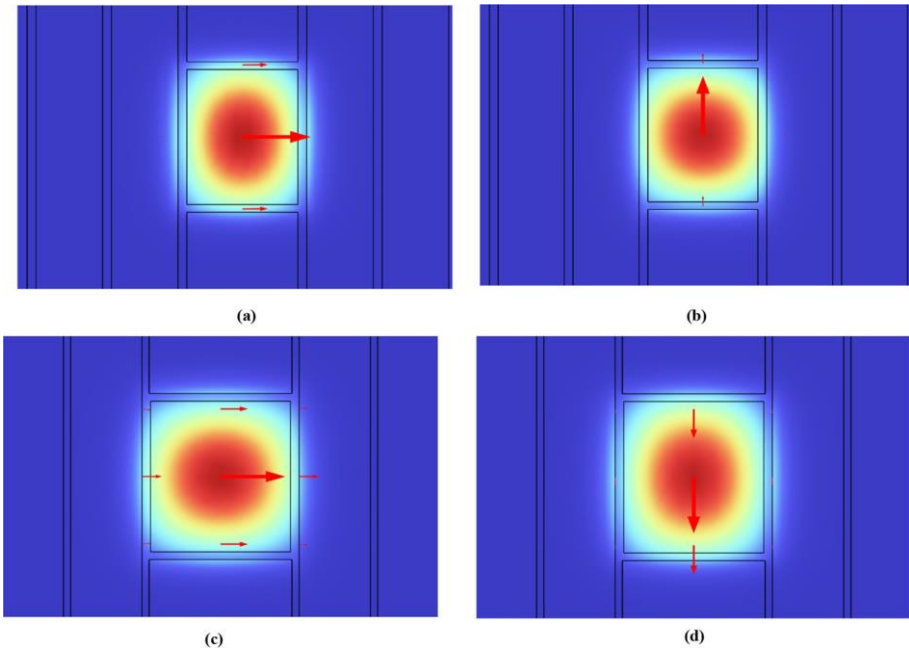
Fig. 2 **a**, **b** Mode electric field distribution and **c**, **d** Mode magnetic field distribution of the proposed fiber for analyte with refractive index 1.39 at 1.4 THz frequency in X and Y polarization direction respectively

rectangular, square, and elliptical air holes can be fabricated using 3D printing and extrusion technologies. Several asymmetrical PCF models have been fabricated by the Max Planck Institute, including elliptical and rectangular designs, demonstrating the successful fabrication of various PCF models (Bulbul et al. 2021). This ensures the feasibility of the fabrication of the suggested PCF fiber.

As the core of the proposed sensor is infiltrated with the analyte. Several infiltration techniques are available for the selective filing of PCF, which include selective filing by collapsing air holes (Xiao et al. 2004), by femtosecond laser micromachining (Wang et al. 2010), by splicing single-mode fiber etc.

4 Numerical analysis

The present study is done on three conditions Optimum (OPT), Optimum +2% (OPT + 2%) and Optimum-2% (OPT − 2%). To attain these conditions core width and height are altered by 2%. The width and height of the core are 400 µm and 500 µm for OPT condition. For OPT + 2% condition the width and height of the core is 408 µm and 510 µm. Similarly, width and height have been set at 392 µm and 490 µm for condition OPT − 2%. Different parameters are evaluated to analyze the performance of the proposed sensor for OPT, OPT + 2%, OPT − 2% conditions. These parameters include Relative sensitivity (RS), confinement loss (*CL*), power fraction (*P*), Non-linearity (γ), Effective mode area (EMA), and Birefringence. These parameters significantly impact the performance of the PCF sensors.

The RS is a crucial property that expresses the change in the optical response of the structure compared to the change in the external parameter. It measures the changes in the RI with the variation in the surroundings. It can be calculated using the following relation (Bulbul et al. 2022):

$$RS = \frac{n}{n_{eff}} \times P$$

(1)

Here, n is the RI of the sensing analyte and n_{eff} is the effective mode index (EMI). Here P represents the power fraction.

Power fraction (P) is the fraction of power located in the core of the fiber. It can be using the following equation (Habib et al. 2019),

$$P = \frac{sample \int R(E_x H_y - E_y H_x)dxdy}{whole \int R(E_x H_y - E_y H_x)dxdy} \times 100\%$$

(2)

Light traveling through the fiber experiences an average refractive index depending upon the design of the PCF. This average RI is called the effective mode index. EMI can be evaluated by Panda and Pukhrambam (2021):

$$n_{eff} = \frac{\beta}{k_o}$$

(3)

ere, β is the normalised propagation constant, k_o represents wave number in vacuum.

Birefringence is also one of the important parameter for designing the PCF sensor as high birefringence in PCF can be used to design sensors that are sensitive to the variation in RI. It describes the difference in refractive index between two perpendicular polarization directions (Yadav et al. 2023). It can be calculated to using,

$$B = |n_{eff}^x - n_{eff}^y|$$

(4)

The optimal region for analyte sensing and the cross-sectional area that interacts with the light is the effective mode area. We can evaluate the effective mode area by the relation:

$$EMA = \frac{\left(\iint |E|^2 dxdy\right)^2}{\iint E^4 dxdy}$$

(5)

Here, $|E|$ denotes the electric field distribution of the proposed fiber sensor.

Confinement loss is an important factor in analyzing the efficiency of an optical device, particularly in photonic crystal fibers. It shows the amount of light leaked within an optical fiber or a waveguide due to inadequate light confinement within the core. Minimum the value of CL better would be the transmission of light within the waveguide.

$$CL\left(\frac{dB}{cm}\right) = 8.868 \times k_o \times l_m(n_{eff}) \times 10^{-2}$$

(6)

Here, k_o is the propagation constant, and $l_m(n_{eff})$ is the imaginary part of the effective refractive index of the propagating fundamental mode.

Non-linearity refers to the modifications in refractive index due to change in light intensity. By altering the parameters, a highly sensitive sensor can be designed to detect even subtle variations in the surrounding medium.

$$Y = \frac{2\pi}{\beta} \frac{n_2}{EMA} \tag{7}$$

where n_2 is non-linear refractive index and EMA is effective mode area.

5 Result and discussion

To assess the guiding characteristics of the suggested rectangular core PCF, simulation and analysis are conducted using the FEM based COMSOL Multiphysics Software. Results for OPT, OPT − 2%, and OPT + 2% are evaluated and compared.

Figure 3 a, b shows OPT condition relative sensitivity variation with frequency for different analytes with RI ranging from n = 1.35 to 1.39. Relative sensitivity for analytes with higher refractive index is greater than for analytes with lower refractive index. We obtained relative sensitivity values 96.889%, 97.217%, 97.515%, 97.787%, 98.035% for RI of the analyte n = 1.35, 1.36, 1.37, 1.38, 1.39 respectively in Y polarized direction at an operating frequency of 1.4 THz. Relative sensitivity values of 97.868%, 98.135%, 98.378%, 98.599%, 98.800% are achieved for analyte with RI n = 1.35, 1.36, 1.37, 1.38, 1.39 respectively in X polarized direction at an operating frequency of 1.4 THz. These values indicate that there is an exceptionally high relative sensitivity obtained to all analyte samples.

Figure 4a, b shows relative sensitivity variation for OPT − 2% for different analytes. We obtained relative sensitivity values 94.997%, 95.481%, 95.921%, 96.321%, and 96.686% for RI of the analyte n = 1.35, 1.36, 1.37, 1.38, 1.39 respectively in Y polarized direction at an operating frequency of 1.4 THz. Relative sensitivity values of 96.05%, 96.478%, 96.864%, 97.213%, 97.529% are achieved for analyte with RI, n = 1.35, 1.36, 1.37, 1.38, 1.39 respectively in X polarized direction at an operating frequency of 1.4 THz. These values indicate that there is an exceptionally high relative sensitivity obtained to all analyte samples.

Figure 5a, b shows relative sensitivity variation for OPT + 2%. We obtained relative sensitivity values 98.312%, 98.528%, 98.726%, 98.906%, 99.07% for RI of the analyte n = 1.35, 1.36, 1.37, 1.38, 1.39 respectively in Y polarized direction at an operating
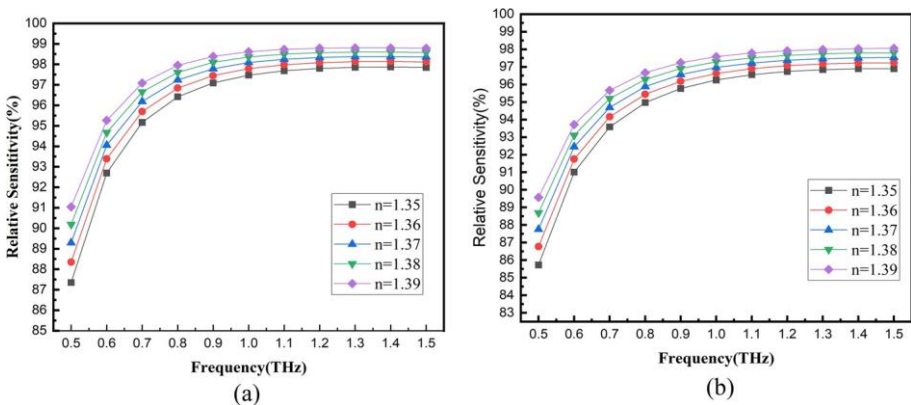

Fig. 3 **a** and **b** Relative sensitivity variation with frequency for OPT case in X and Y polarization directions respectively
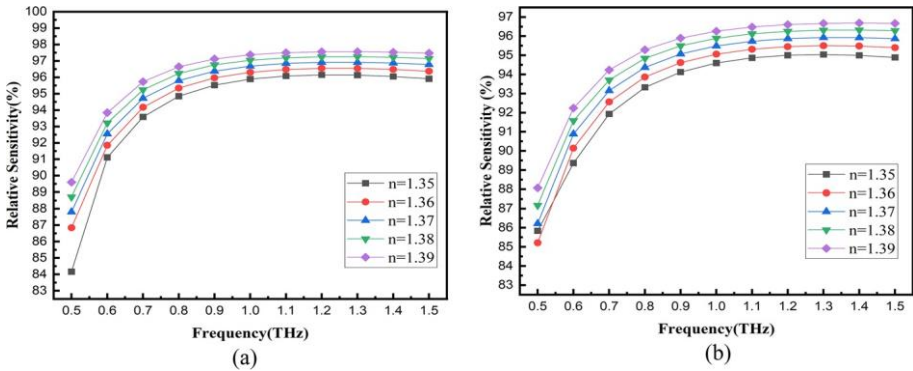
Fig. 4 **a** and **b** Relative sensitivity variation with frequency for OPT−2% case in X and Y polarization directions respectively
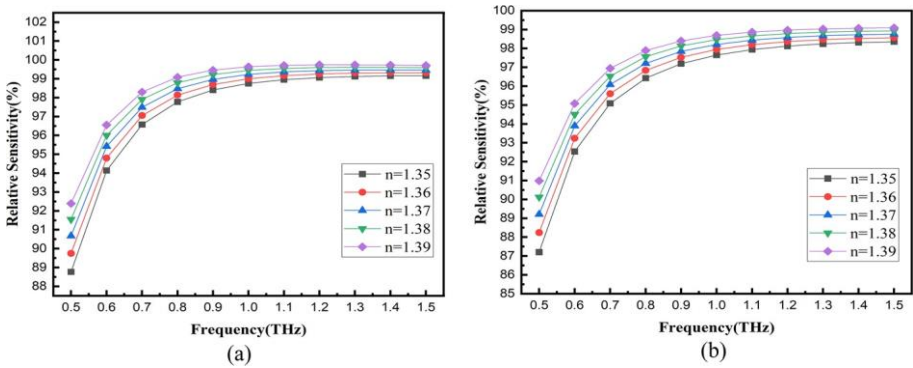

Fig. 5 **a** and **b** Relative sensitivity variation with frequency for OPT+2% case in X and Y polarization directions respectively

frequency of 1.4 THz. Relative sensitivity values of 99.149%, 99.315%, 99.466%, 99.604%, 99.730% are achieved for analyte with RI, n = 1.35, 1.36, 1.37, 1.38, 1.39 respectively in X polarized direction at an operating frequency of 1.4 THz. These values indicate that there is an exceptionally high relative sensitivity obtained to all analyte samples.

Figure 6a–c shows birefringence of different analytes with RI, n = 1.35, 1.36, 1.37, 1.38, 1.39 for OPT, OPT + 2%, OPT − 2% condition. Birefringence decreases with increase in frequency. Birefringence values achieved for analytes with RI, n = 1.35, 1.36, 1.37, 1.38, 1.39 are 0.0015, 0.0015, 0.0014, 0.0014 and 0.0013 for OPT case; 0.0015, 0.0015, 0.0015, 0.0014, and 0.0013 for OPT − 2% case; 0.0014, 0.0013, 0.0013, 0.0013, 0.0012 for OPT + 2% case respectively at 1.4 THz operating frequency.

Figure 7a, b shows the EMA profile achieved for different analytes within the 1.35–1.39 RI range for X and Y polarization directions. With the increase in the frequency of light, there is a decrease in the EMA of the fiber. Higher frequencies mean shorter wavelengths and shorter wavelengths can be easily confined in the fiber. Furthermore, the fiber's waveguide dispersion becomes more prominent at higher frequencies, which leads to the tight confinement of light inside the fiber's core (Ferdous et al. 2022; Almawgani et al.
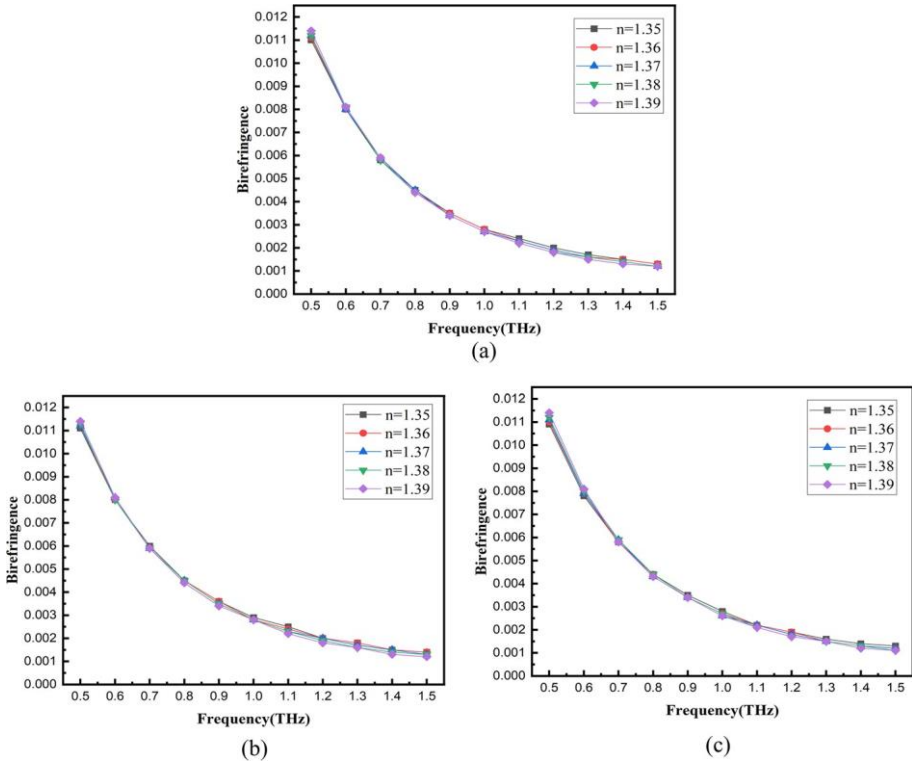
Fig.6 a, b, and **c** Birefringence variation with frequency for OPT, OPT−2%, OPT+2% respectively
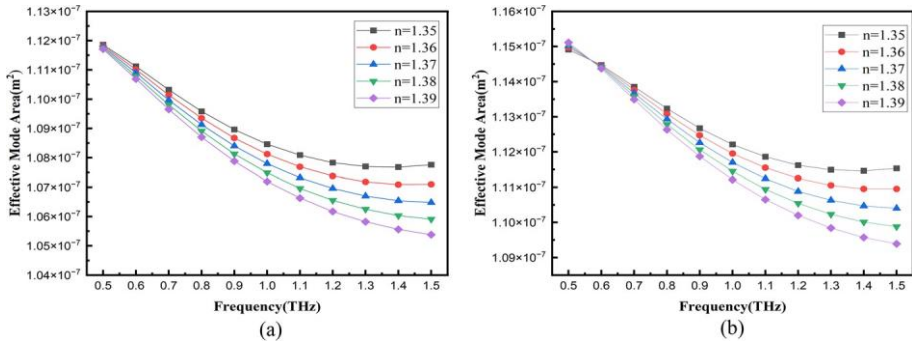

Fig. 7 a and **b** Effective mode area variation with frequency for OPT case in X and Y polarization directions respectively

2023). For OPT condition we achieved an average effective mode area of order 10^{-7} m². At 1.4 THz frequency effective mode area is 1.1146 10^{-7} m², 1.1095 10^{-7} m², 1.1047 10^{-7} m², 1.1001 10^{-7} m², 1.0957 10^{-7} m² for an analyte with RI, n=1.35, 1.36, 1.37, 1.38, 1.39 respectively with Y polarization of electric field. In X polarized direction we observed an effective mode area of 1.0768 10^{-7} m², 1.0709 10^{-7} m², 1.0654 10^{-7} m²,
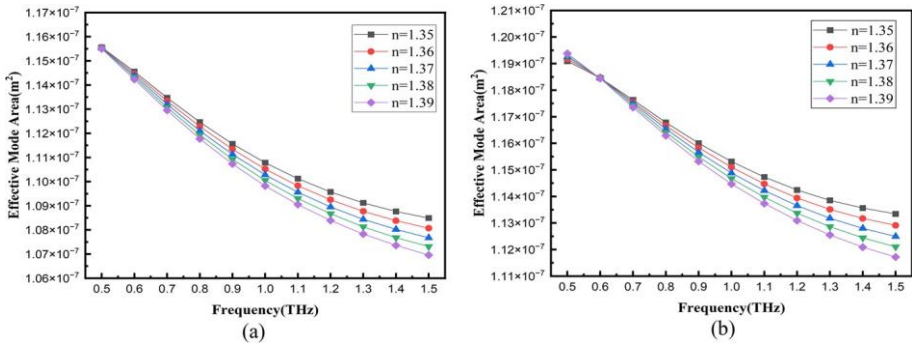
Fig. 8 **a** and **b** Effective mode area variation with frequency for OPT− 2% case in X and Y polarization directions respectively
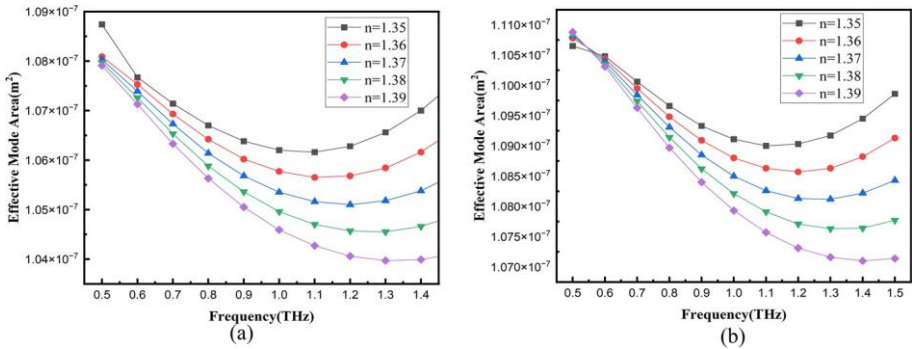

Fig. 9 **a** and **b** Effective mode area variation with frequency for OPT+ 2% case in X and Y polarization directions respectively

1.0603×10^{-7} m², 1.0556×10^{-7} m² for an analyte with RI, n = 1.35, 1.36, 1.37, 1.38, 1.39 respectively.

Figure 8a, b represents EMA for OPT − 2% condition. For 1.4 THz frequency effective mode area is 1.0945×10^{-7} m², 1.0882×10^{-7} m², 1.0822×10^{-7} m², 1.0764×10^{-7} m², 1.0710×10^{-7} m² for an analyte with RI, n = 1.35, 1.36, 1.37, 1.38, 1.39 respectively with Y polarization of electric field. In X polarized direction we observed an effective mode area of 1.0700×10^{-7} m², 1.0616×10^{-7} m², 1.0538×10^{-7} m², 1.0466×10^{-7} m², 1.0399×10^{-7} m² for an analyte with RI, n = 1.35, 1.36, 1.37, 1.38, 1.39 respectively.

Figure 9a, b shows variation of EMAfor OPT + 2% condition for different analytes. At 1.4 THz frequency effective mode area is 1.1356×10^{-7} m², 1.1317×10^{-7} m², 1.1280×10^{-7} m², 1.1244×10^{-7} m², 1.204×10^{-7} m² for an analyte with RI, n = 1.35, 1.36, 1.37, 1.38, 1.39 respectively with Y polarization of electric field. In X polarized direction we observed an effective mode area of 1.0876×10^{-7} m², 1.0838×10^{-7} m², 1.0802×10^{-7} m², 1.0768×10^{-7} m², 1.0736×10^{-7} m² for an analyte with RI, n = 1.35, 1.36, 1.37, 1.38, 1.39 respectively.

Figure 10a, b shows the non-linearity variation for OPT condition for both X and Y polarization directions in frequency range of 0.5–1.5 THz. Non-linearity increases linearly with frequency. We achieved non-linearity values of 5.528×10^{-9} W⁻¹ m⁻¹,
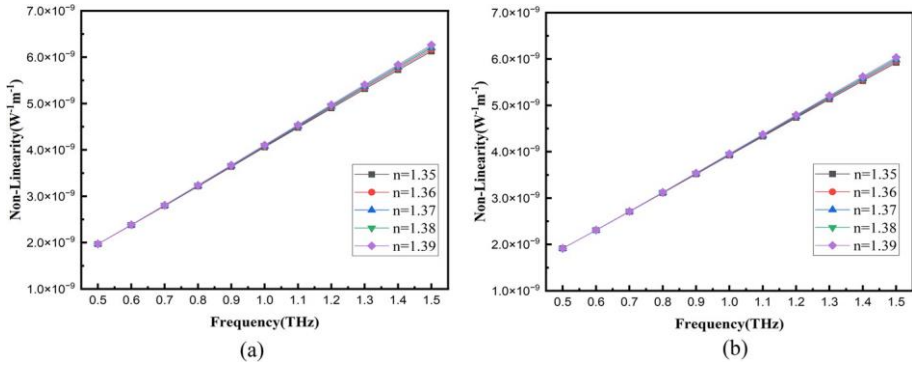
Fig. 10 **a** and **b** Non-Linearity variation with frequency for OPT case in X and Y polarization directions respectively

5.553×10^{-9} W^{-1} m^{-1}, 5.557×10^{-9} W^{-1} m^{-1}, 5.601×10^{-9} W^{-1} m^{-1}, 5.623×10^{-9} W^{-1} m^{-1} for RI of sensing analyte, n = 1.35, 1.36, 1.37, 1.38, 1.39 respectively in Y polarized direction at 1.4 THz frequency. Non-linearity values of 5.72×10^{-9} W^{-1} m^{-1}, 5.753×10^{-9} W^{-1} m^{-1}, 5.783×10^{-9} W^{-1} m^{-1}, 5.811×10^{-9} W^{-1} m^{-1}, 5.837×10^{-9} W^{-1} m^{-1} were achieved for RI of sensing analyte n = 1.35, 1.36, 1.37, 1.38, 1.39 respectively in X polarized direction at 1.4 THz operating frequency.

As shown in Fig. 11a, b which is OPT − 2% condition we achieved non-linearity values of 5.6297×10^{-9} W^{-1} m^{-1}, 5.6624×10^{-9} W^{-1} m^{-1}, 5.6939×10^{-9} W^{-1} m^{-1}, 5.67242×10^{-9} W^{-1} m^{-1}, 5.7533×10^{-9} W^{-1} m^{-1} for RI of sensing analyte, n = 1.35, 1.36, 1.37, 1.38, 1.39 respectively in Y polarized direction at 1.4THz frequency. Non-linearity values of 5.7587×10^{-9} W^{-1} m^{-1}, 5.8041×10^{-9} W^{-1} m^{-1}, 5.8470×10^{-9} W^{-1} m^{-1}, 5.8875×10^{-9} W^{-1} m^{-1}, 5.9255×10^{-9} W^{-1} m^{-1} were achieved for RI of sensing analyte n = 1.35, 1.36, 1.37, 1.38, 1.39 respectively in X polarized direction at 1.4 THz operating frequency.

In Fig. 12a, b, for OPT + 2% condition non-linear coefficient values of 5.4262×10^{-9} W^{-1} m^{-1}, 5.4448×10^{-9} W^{-1} m^{-1}, 5.4628×10^{-9} W^{-1} m^{-1},
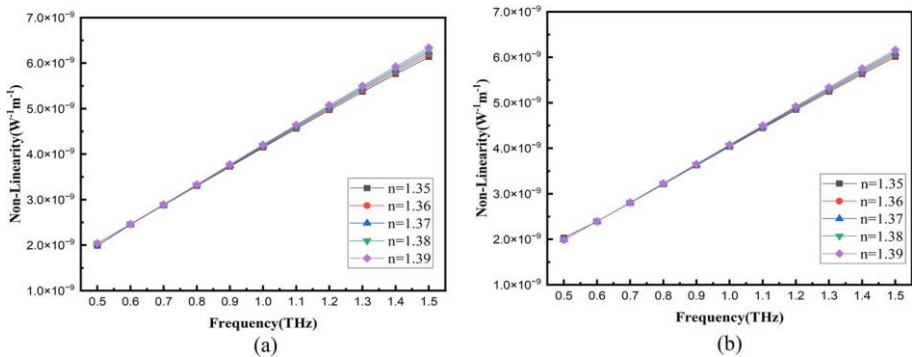

Fig. 11 **a** and **b** Non-Linearity variation with frequency for OPT− 2% case in X and Y polarization directions respectively
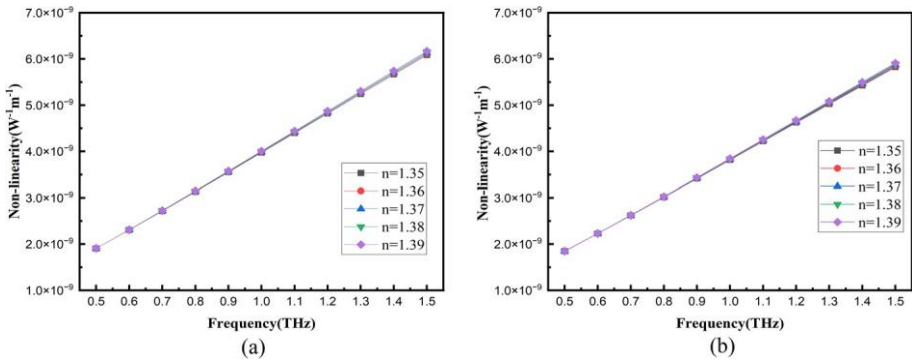
Fig. 12 **a** and **b** Non-Linearity variation with frequency for OPT + 2% case in X and Y polarization directions respectively

5.4801×10^{-9} W^{-1} m^{-1}, 5.4970×10^{-9} W^{-1} m^{-1} for RI of sensing analyte, n = 1.35, 1.36, 1.37, 1.38, 1.39 respectively in Y polarized direction at 1.4 THz frequency are achieved. Non-linear coefficient values of 5.6653×10^{-9} W^{-1} m^{-1}, 5.6854×10^{-9} W^{-1} m^{-1}, 5.7043×10^{-9} W^{-1} m^{-1}, 5.7223×10^{-9} W^{-1} m^{-1}, 5.7394×10^{-9} W^{-1} m^{-1} were achieved for RI of sensing analyte n = 1.35, 1.36, 1.37, 1.38, 1.39 respectively in X polarized direction at 1.4 THz operating frequency.

Figure 13a, b shows OPT condition CL variation for both X and Y polarization directions in the 0.5–1.5 THz frequency range. The CL graph depicts that confinement loss decreases as frequency increases. The confinement of lights gets better with larger frequencies as larger frequencies correspond to shorter wavelengths and shorter wavelengths are easier to confine within the fiber's periodic structure, the CL decreases for larger frequencies. Further with increase in frequency, the waveguide dispersion within the fiber becomes increasingly significant, which results in a more pronounced confinement of light within the core (Yadav et al. 2023). We observed the CL of 8.409×10^{-15} dB/cm, 8.659×10^{-15} dB/cm, 3.559×10^{-14} dB/cm, 3.849×10^{-14} dB/cm, 5.639×10^{-14} dB/cm for RI of analyte, n = 1.35, 1.36, 1.37, 1.38, 1.39 respectively in Y polarized direction at 1.4 THz frequency. In X polarized direction we observed CL
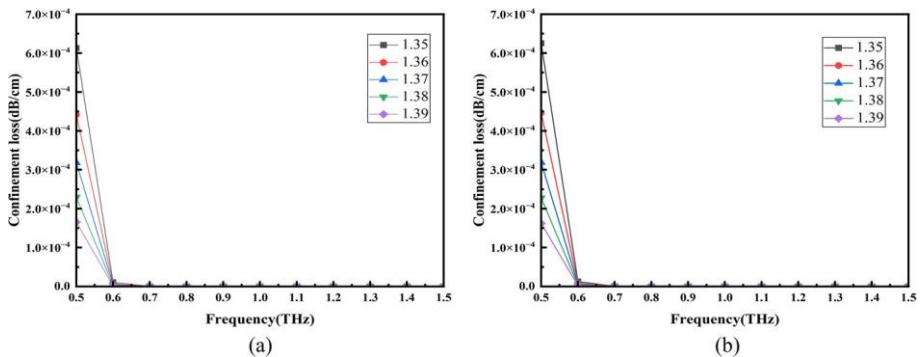

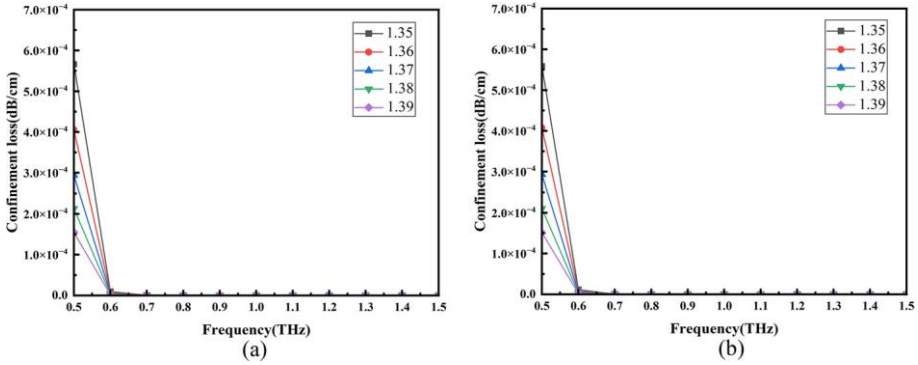**Fig. 13** **a** and **b** Confinement Loss variation with frequency for OPT case in X and Y polarization directions respectively

Fig. 14 **a** and **b** Confinement Loss variation with frequency for OPT − 2% case in X and Y polarization directions respectively
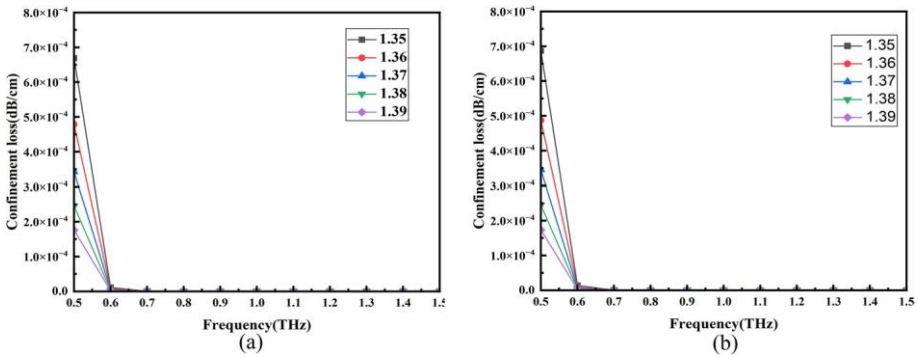

Fig. 15 **a** and **b** Confinement Loss variation with frequency for OPT− 2% case in X and Y polarization directions respectively

of 2.779×10^{-14} dB/cm, 2.489×10^{-16} dB/cm, 1.499×10^{-13} dB/cm, 7.479×10^{-14} dB/cm, 1.759×10^{-14} dB/cm for the RI of analyte, n = 1.35, 1.36, 1.37, 1.38, 1.39 respectively at 1.4 THz frequency.

Figure 14a, b shows variation of CL for OPT − 2% condition for which we achieved CL of 7.18×10^{-15} dB/cm, 1.51×10^{-14} dB/cm, 5.51×10^{-14} dB/cm, 9 .00× 10^{-14} dB/cm, 2.54×10^{-14} dB/cm for RI of analyte, n = 1.35, 1.36, 1.37, 1.38, 1.39 respectively in Y polarized direction at 1.4 THz frequency. In X polarized direction we observed CL of 1.49×10^{-14} dB/cm, 9.56×10^{-13} dB/cm, 6.26×10^{-14} dB/cm, 6.55×10^{-14} dB/cm, 3.67×10^{-14} dB/cm for RI of analyte, n = 1.35, 1.36, 1.37, 1.38, 1.39 respectively at 1.4 THz frequency.

Figure 15a, b represents confinement loss profile for OPT + 2% condition for which we achieved confinement loss of 6.53×10^{-14} dB/cm, 7.58×10^{-14} dB/cm, 9.62×10^{-14} dB/cm, 9.74×10^{-15} dB/cm, 1.48×10^{-13} dB/cm for refractive index of analyte, n = 1.35, 1.36, 1.37, 1.38, 1.39 respectively in Y polarized direction at 1.4 THz frequency. In X polarized direction we observed confinement loss of 4.71×10^{-14} dB/cm, 1.68×10^{-14} dB/cm, 8.51×10^{-14} dB/cm, 5.05×10^{-14} dB/cm, 2.97×10^{-15} dB/cm for refractive index of analyte, n = 1.35, 1.36, 1.37, 1.38, 1.39 respectively at 1.4 THz frequency.
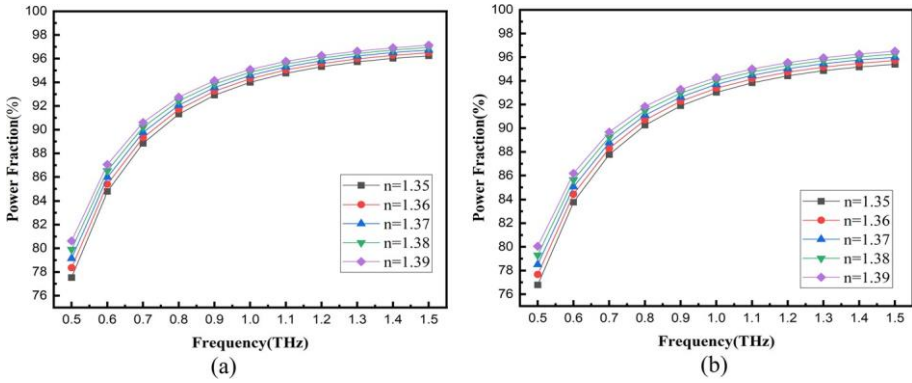
Fig. 16 **a** and **b** Power fraction variation with frequency for OPT case in X and Y polarization directions respectively
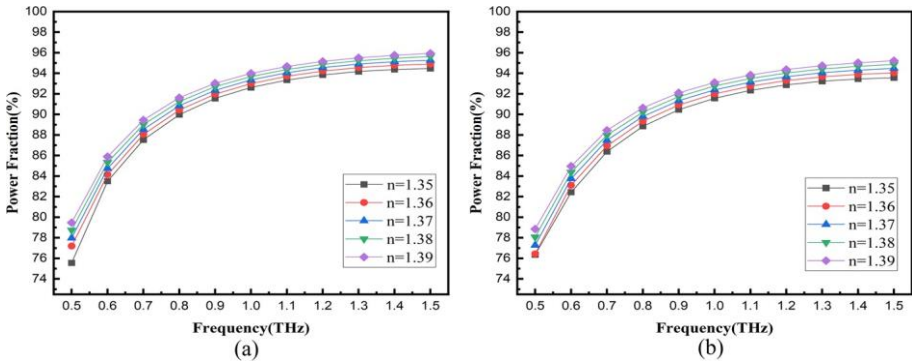

Fig. 17 **a** and **b** Power Fraction variation with frequency for OPT−2% case in X and Y polarization directions respectively

Figure 16a, b shows variation of power fraction of different analytes in X and Y polarized directions for OPT condition. One of the key factors influencing the sensor's performance is its sensitivity which is determined by Power fraction. The graph shows that core power fraction is generally more for analyte with higher refractive index. The values of power fraction have been achieved are 95.169%, 95.479%, 95.762%, 96.021%, 95.259% for RI of analyte n = 1.35, 1.36, 1.37, 1.38, 1.39 respectively in Y polarized direction at 1.4 THz frequency. We also observed power fraction values as 96.023%, 96.277%, 96.509%, 96.722%, 96.917% for RI of analyte n = 1.35, 1.36, 137, 1.38, 1.39 respectively in X polarized direction at operating frequency of 1.4 THz.

Figure 17a, b represents power fraction values for the OPT − 2% condition. Power fraction values have been achieved are 93.445%, 93.894%, 94.304%, 94.678%, 95.020% for RI of analyte n = 1.35, 1.36, 1.37, 1.38, 1.39 respectively in Y polarized direction at 1.4THz frequency. We also observed power fraction values as 94.368%, 94.766%, 95.128%, 95.455%, 95.753% for RI of analyte n = 1.35, 1.36, 137, 1.38, 1.39 respectively in X polarized direction at operating frequency of 1.4 THz.

Figure 18a, b shows power fraction values for OPT +2% and we achieved power fraction values of 96.457%, 96.668%, 96.862%, 97.040%, 97.204% for RI of analyte n = 1.35, 1.36, 1.37, 1.38, 1.39 respectively in Y polarized direction at 1.4 THz frequency. We also observed power fraction values as 97.176%, 97.341%, 97.493%, 96.633%, 97.763% for RI of analyte n = 1.35, 1.36, 137, 1.38, 1.39 respectively in X polarized direction at operating frequency of 1.4 THz.

Table 1 shows the comparison between model suggested in this paper with previously suggested models in THz regime. The proposed design is a general-purpose sensor for bio sensing application which is capable of sensing different analytes with refractive index ranging from n = 1.35 to 1.39. Various analytes like Red blood cells, cancer cells have their refractive indices falling in RI range of 1.35–1.39, so the proposed detector is capable of detecting all these analytes. We have achieved better results than previously cited work with a design that is more sensitive to the RI change than many previously proposed designs.

6 Conclusion

In this paper, a rectangular core PCF sensor has been proposed for sensing different analyte with refractive index ranging from 1.35–1.39. The cladding is composed of rectangular shaped air holes. Zeonex is used as fiber material. The proposed refractive index fiber sensor can be utilized for detection of many biological components such as blood components (RBC, WBC, Plasma etc.), various cancer cells etc. The proposed sensor shows a very high relative sensitivity of 98.8% and 98.035% for an analyte of refractive index 1.39 at 1.4 THz operating frequency in X and Y polarized direction respectively. Besides CL is noticed only 7.75×10^{-14} dB/cm and 5.627×10^{-14} dB/cm in X and Y polarized direction respectively for an analyte of refractive index 1.39. Furthermore, other optical properties such as effective refractive index, EMA, and Non-linearity have been achieved. Table 2 shows values of different parameters for optimization conditions OPT, OPT − 2%, OPT + 2%. It is possible to build the suggested PCF using the current fabrication techniques. The proposed model has demonstrated a preference for being satisfactory in detecting various analytes.
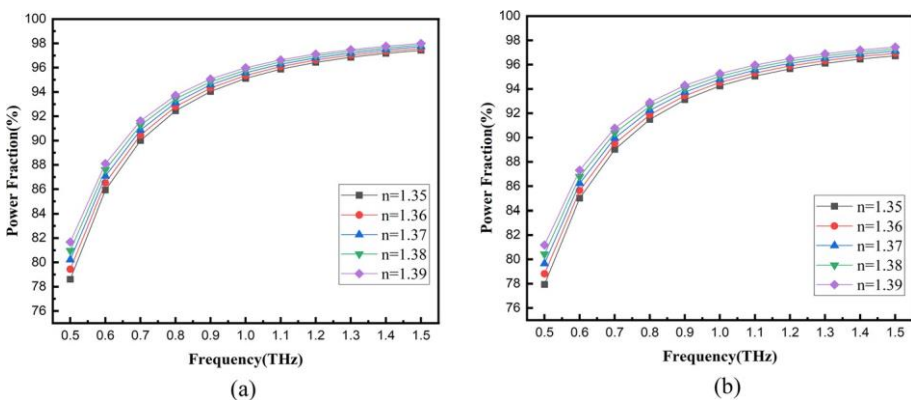

Fig. 18 a and **b** Power Fraction variation with frequency for OPT +2% case in X and Y polarization directions respectively

Table 1 Comparison of proposed fiber with existing photonic crystal fiber sensors

References	Detection target	Operating frequency (THz)	Background material	Effective mode area	Relative sensitivity (%)	Confinement loss
Hossain et al. (2020)	Blood components (RBCs)	1.5	Topas	1.55×10^5 µm^2	80.93	–
Haddad et al. (2013)	Chemical (water)	1.6	Topas	1.57×10^5 µm^2	–	1.06×10^{-9} cm^{-1}
Binti Suhaimi et al. (2020)	Chemical (liquid cocaine)	1	Zeonex	1.11×10^5 µm^2	87.02	9.42×10^{-4} cm^{-1}
Mohammed et al. (2023)	Biosensor(tuberculosis)	2.2	Zeonex	4.342×10^{-8} m^2	90.60	3.13×10^{-9} cm^{-1}
This work	Biosensor	1.4	Zeonex	1.0559×10^{-7} m^2	98.80	1.759×10^{-14} dB/cm

Table 2 Different parameters for OPT, OPT −2% and OPT +2% cases at 1.4 THz for analayte with refractive index n = 1.39 in Y and X Polarization direction

Model	Analyte	Effective mode index		Effective mode area (m^2)		Non-linearity ($W^{-1}\,m^{-1}$)		Relative sensitivity (%)	
		Y	X	Y	X	Y	X	Y	X
OPT	n = 1.39	1.3648	1.3635	1.10×10^{-7}	1.06×10^{-7}	5.62×10^{-9}	5.84×10^{-9}	98.035	98.8
OPT −2%	n = 1.39	1.366	1.3647	1.07×10^{-7}	1.04×10^{-7}	5.75×10^{-9}	5.93×10^{-9}	96.686	97.529
OPT +2%	n = 1.39	1.3638	1.3626	1.12×10^{-7}	1.07×10^{-7}	5.50×10^{-9}	5.74×10^{-9}	99.07	99.73

The investigated PCF provides interesting findings and may find use in bio-sensing application. The proposed sensor can be easily fabricated with the help of the existing fabrication technology.

Declarations

References

Ahmed, K., Ahmed, F., Roy, S., et al.: Refractive index-based blood components sensing in terahertz spectrum. IEEE Sens. J. **19**, 3368–3375 (2019). https://doi.org/10.1109/JSEN.2019.2895166

Almawgani, A.H.M., Alhamss, D.N., Taya, S.A., et al.: Theoretical analysis of a refractive index sensor based on a photonic crystal fiber with a rectangular core. Opt. Quantum Electron. (2023). https://doi.org/10.1007/s11082-023-05172-2

Arif, M.F.H., Ahmed, K., Asaduzzaman, S., Azad, M.A.K.: Design and optimization of photonic crystal fiber for liquid sensing applications. Photonic Sens. **6**, 279–288 (2016). https://doi.org/10.1007/s13320-016-0323-y

Bao, H., Nielsen, K., Rasmussen. H. K. et al.: Fabrication and experimental characterization. (2010)

Binti Suhaimi, N.A.N., Yakasai, I.K., Abas, E., et al.: Modelling and simulation of novel liquid-infiltrated PCF biosensor in terahertz frequencies. IET Optoelectron. **14**, 411–416 (2020). https://doi.org/10.1049/iet-opt.2020.0069

Bise, R. T., Trevor, D. J.: Sol-gel derived microstructured fiber: fabrication and characterization. In: Optical fiber communication conference, vol. 3, p. 3. Optical Society of America, Anaheim (2005)

Bulbul, A.A.M., Kouzani, A.Z., Mahmud, M.A.P., Al, N.A.: Design and numerical analysis of a novel rectangular PCF (R-PCF)-based biochemical sensor (BCS) in the THz regime. Int. J. Opt. (2021). https://doi.org/10.1155/2021/5527724

Bulbul, A.A.M., Rahaman, H., Podder, E.: Design and quantitative analysis of low loss and extremely sensitive PCF-based biosensor for cancerous cell detection. Opt. Quantum Electron. (2022). https://doi.org/10.1007/s11082-022-03513-1

Ebendorff-Heidepriem, H., Schuppich, J., Dowler, A., et al.: 3D-printed extrusion dies: a versatile approach to optical material processing. Opt. Mater. Express **4**, 1494 (2014). https://doi.org/10.1364/ome.4.001494

Ekhlasur Rahaman, M., Bellal Hossain, M., Shekhar Mondal, H. et al.: Highly sensitive photonic crystal fiber liquid sensor in terahertz frequency range. In: Materials today: proceedings, pp. 3815–3820. Elsevier (2020)

Ferdous, A.H.M.I., Anower, M.S., Musha, A., et al.: A heptagonal PCF-based oil sensor to detect fuel adulteration using terahertz spectrum. Sens. Biosensing. Res. (2022). https://doi.org/10.1016/j.sbsr.2022.100485

Ghazanfari, A., Li, W., Leu, M.C., Hilmas, G.E.: A novel freeform extrusion fabrication process for producing solid ceramic components with uniform layered radiation drying. Addit. Manuf. **15**, 102–112 (2017). https://doi.org/10.1016/j.addma.2017.04.001

Habib, M.A., Anower, M.S., Abdulrazak, L.F., Reza, M.S.: Hollow core photonic crystal fiber for chemical identification in terahertz regime. Opt. Fiber Technol. (2019). https://doi.org/10.1016/j.yofte.2019.101933

El Haddad, J., Bousquet, B., Canioni, L., Mounaix, P.: Review in terahertz spectral analysis. TrAC—Trends Anal. Chem. **44**, 98–105 (2013)

Hossain, M.B., Podder, E.: Design and investigation of PCF-based blood components sensor in terahertz regime. Appl. Phys. A Mater. Sci. Process. (2019). https://doi.org/10.1007/s00339-019-3164-x

Hossain, M.B., Podder, E., Bulbul, A.A.M., Mondal, H.S.: Bane chemicals detection through photonic crystal fiber in THz regime. Opt. Fiber Technol. (2020). https://doi.org/10.1016/j.yofte.2019.102102

Islam, M.S., Sultana, J., Rifat, A.A., et al.: Terahertz sensing in a hollow core photonic crystal fiber. IEEE Sens. J. **18**, 4073–4080 (2018). https://doi.org/10.1109/JSEN.2018.2819165

Mohammed, N.A., Khedr, O.E., El-Rabaie, E.S.M., Khalaf, A.A.M.: High-sensitivity early detection biomedical sensor for tuberculosis with low losses in the terahertz regime based on photonic crystal fiber technology. Photonic Sens. (2023). https://doi.org/10.1007/s13320-023-0675-z

Panda, A., Pukhrambam, P.D.: Design and analysis of porous core photonic crystal fiber based ethylene glycol sensor operated at infrared wavelengths. J. Comput. Electron. **20**, 943–957 (2021). https://doi.org/10.1007/s10825-020-01650-y

Rahaman, M.E., Jibon, R.H., Mondal, H.S., et al.: Design and optimization of a PCF-based chemical sensor in THz regime. Sens. Biosens. Res. (2021). https://doi.org/10.1016/j.sbsr.2021.100422

Selim Hossain, M., Sen, S.: Design and performance improvement of optical chemical sensor based photonic crystal fiber (PCF) in the terahertz (THz) wave propagation. SILICON (2021). https://doi.org/10.1007/s12633-020-00696-8/Published

Sultana, J., Islam, Md.S., Ahmed, K., et al.: Terahertz detection of alcohol using a photonic crystal fiber sensor. Appl. Opt. **57**, 2426 (2018). https://doi.org/10.1364/ao.57.002426

Wang, Y., Liao, C.R., Wang, D.N.: Femtosecond laser-assisted selective infiltration of microstructured optical fibers. Opt. Express **18**(17), 18056–18060 (2010)

Xiao, L., Jin, W., Demokan, M.S., et al.: Fabrication of selective injection microstructured optical fibers with a conventional fusion splicer. Opt. Express **13**(22), 9014–9022 (2004)

Yadav, S., Lohia, P., Dwivedi, D.K.: A novel approach for identification of cancer cells using a photonic crystal fiber-based sensor in the terahertz regime. Plasmonics **18**, 1753–1769 (2023). https://doi.org/10.1007/s11468-023-01887-w